Ages of lunar impact breccias: limits for timing of the Imbrium impact

Alexander A. Nemchin[1, 2], Tao Long[1, 3, 4], Bradley L. Jolliff[5], Yusheng Wan[1, 3], Joshua F. Snape[6], Ryan Zeigler[7], Marion L. Grange[6], Dunyi Liu[1, 3, 4], Martin J. Whitehouse[6], Nicholas E. Timms[2], Fred Jourdan[2]

[1] *Institute of Geology, Chinese Academy of Geological Sciences, Beijing, China*

[2] *School of Earth and Planetary Sciences, Curtin University, Perth, GPO Box U1987, WA 6845, Australia*

[3] *Beijing SHRIMP Center, Beijing, China*

[4] *Shandong Institute of Geological Sciences, Jinan, China*

[5] *Department of Earth and Planetary Sciences and The McDonnell Center for the Space Sciences, Washington University in St. Louis, One Brookings Drive, St. Louis, MO, USA*

[6] *Department of Geosciences, Swedish Museum of Natural History, SE-104 05 Stockholm, Sweden.*

[7] *Johnson Space Centre, NASA, 1601 NASA Pkwy, Houston, TX 77958, USA*

Corresponding author:

Alexander Nemchin
Curtin University
Kent Str., Bentley, Perth, Western Australia 6102
Email: a.nemchin@curtin.edu.au
Phone: +61 9266 7979
Mobile: +61 406785877

Abstract

Since the Apollo 14 mission delivered samples of the Fra Mauro formation, interpreted as ejecta of the Imbrium impact, defining the age of this impact has emerged as one of the critical tasks required for the complete understanding of the asteroid bombardment history of the Moon and, by extension, the inner Solar System. Significant effort dedicated to this task has resulted in a substantial set of ages centered around 3.9 Ga and obtained for the samples from most Apollo landing sites using a variety of chronological methods. However, the available age data are scattered over a range of a few tens of millions of years, which hinders the ability to distinguish between the samples that are truly representative of the Imbrium impact and those formed/reset by other, broadly contemporaneous impact events. This study presents a new set of U-Pb ages obtained for the VHK (very high K) basalt clasts found in the Apollo 14 breccia sample 14305 and phosphates from (i) several fragments of impact-melt breccia extracted from Apollo 14 soil sample 14161, and (ii) two Apollo 15 breccias 15455 and 15445. The new data obtained for the Apollo 14 samples increase the number of independently dated samples from this landing site to ten. These Apollo 14 samples represent the Fra Mauro formation, which is traditionally viewed as Imbrium ejecta, and therefore should record the age of the Imbrium impact. Using the variance of ten ages, we propose an age of 3922±12 Ma for this event. Samples that yield ages within these limits can be considered as possible products of the Imbrium impact, while those that fall significantly outside this range should be treated as representing different impact events. Comparison of this age for Imbrium (determined from Apollo 14 samples) with the ages of another eleven impact-melt breccia samples collected at four other landing sites and a related lunar meteorite suggests that they can be viewed as part of Imbrium ejecta. Comprehensive review of $^{40}Ar/^{39}Ar$ ages available for impact melt samples from different landing sites and obtained using the step-heating technique, suggests that the majority of the samples that gave robust plateau ages are indistinguishable within uncertainties and altogether yield a weighted average age of 3916 ± 7 Ma (95 % conf., MSWD = 1.1; P =0.13) and a median average age of 3919 +14/-12 Ma, both of which agree with the confidence interval obtained using the U-Pb system. These samples, dated by $^{40}Ar/^{39}Ar$ method, can be also viewed as representing the Imbrium impact. In total 36 out of 41 breccia samples from five landing sites can be interpreted to represent formation of the Imbrium basin, supporting the conclusion that Imbrium material was distributed widely across the near side of the Moon. Establishing temporal limits for the Imbrium impact allows discrimination of ten samples with Rb-Sr and

61 $^{40}Ar/^{39}Ar$ ages about 50 Ma younger than 3922±12 Ma. This group may represent a separate
62 single impact on the Moon and needs to be investigated further to improve our understanding
63 of lunar impact history.

64

65 **1. Introduction.**

66 Understanding of the impact history of the Moon is one of the most profound tasks of
67 planetary research as it forms an integral part of any comprehensive model describing the
68 history of the inner Solar System. The Moon and other planetary bodies preserve a broadly
69 defined account of the impact record, indicating an overall decay in the flux of impactors in
70 the Solar System through time, with a possibility of one (Turner et al., 1973) or several
71 (Fischer-Gödde and Becker, 2012; Fernandes et al., 2013; Hopkins and Mojzsis, 2015) spikes
72 at specific time intervals. One of the most widely discussed and hotly debated hypotheses is
73 the proposed period of high impact rate around 3.9 Ga known as the Late Heavy
74 Bombardment (LHB; Turner et al., 1973; Tera et al., 1974; Ryder, 1990; Bottke and Norman,
75 2017). Support for the LHB model originated from very early K-Ar dating as well as Rb-Sr
76 and U-Pb data obtained for Apollo samples (Turner et al., 1973; Tera et al., 1974).
77 Nevertheless, discussions of the LHB model have reached a stalemate owing to the general
78 lack of reliable links between absolute ages and impact events, in particular, those ages that
79 can be confidently linked to a specific impact basin on the Moon whose stratigraphic position
80 is unambiguous (e.g., Spudis et al., 2011).

81 Early work on Apollo samples (e.g., Tera et al., 1974) led to the interpretation that a sharp,
82 short-lived spike in large impacts, named the Terminal Lunar Cataclysm, occurred around
83 3.9-4.0 Ga. In contrast, some workers advocate a gentler peak in the flux of impactors
84 distributed over several hundred million years (e.g., Bottke and Norman, 2017). In addition, a
85 possibility of monotonous exponential decay of the flux has also been discussed by some
86 authors as a viable alternative (e.g. Fritz et al., 2014). Addressing this controversy from the
87 lunar perspective is complicated by the areal coverage of currently available lunar samples
88 with known provenance, which have been collected from a somewhat restricted region on the
89 near side of the Moon and could be biased by the signatures of the impacts closest to this area
90 (e.g., Warren et al., 2005). In fact, the existing chronological data obtained from the lunar
91 samples may indicate that many of the accessible materials have been influenced to some
92 degree by a single impact event, which is believed to have been the Imbrium basin-forming

impact event (e.g., Haskin et al., 2003; Baldwin, 2006). However, general scatter of the obtained ages in the range of about 20-30 Ma (sometimes more) precludes precise and accurate dating of even this single impact. This scatter in the data reflects: (i) disagreement between the ages of samples with proposed similarity of origin when analyzed by the same radiometric system, (ii) disagreement between the ages of different fragments from the same samples, and (iii) apparent disagreement between two chronological systems (U-Pb and $^{40}Ar/^{39}Ar$) most widely used to determine ages of relevant samples. The latter was proposed to be related to discrepancy in decay constants in several studies (e.g. Norman et al. 2006; Liu et al., 2012), but has not been fully investigated by recalculation of published $^{40}Ar/^{39}Ar$ data using updated decay constants and irradiation monitor ages.

Reaching agreement with respect to the timing of the Imbrium impact (and its uncertainty) is an important step forward in pursuing an overall goal of understanding lunar impact history because it will provide a basis for a clear distinction of age data that represent different events. Consequently, the aim of this manuscript is to discuss current progress and difficulties related to the dating of the Imbrium basin and propose a best currently possible estimate of its age based on newly obtained and published U-Pb data for a range of samples from five Apollo landing sites. Even if assigning a specific age to Imbrium basin with full degree of confidence may not be possible owing to the difficulty in unambiguously linking collected samples to specific impacts, establishing a systematic approach for distinguishing samples that can be interpreted as originating from different impacts will advance our understanding of lunar impact history.

Defining the age of an impact can be done by either analyzing rocks representing cooled impact melt (i.e., material that is mostly devoid of mineral and lithic fragments inherited from the target rocks) or impact melt-breccias (sometimes containing impact melt as matrix, but also containing fragmented target rocks), with the former appearing to be least ambiguous with respect to the age interpretation, although outgassing of Ar from digested clasts into impact melt can produce unexpected effects that can significantly affect results using the $^{40}Ar/^{39}Ar$ isotope system (e.g. Jessberger et al., 1975; Mercer et al., 2019). Impact melt can be found as an isolated component, almost free of the fragments, in some Apollo samples, for example in 15445 and 15455 investigated here and proposed as the best potential representatives of Imbrium impact melt (e.g., Ryder and Spudis, 1987). However, samples of clast-free impact-melt rocks that can be unambiguously linked to the Imbrium basin formation or impacts that generated other basins on the Moon are absent in lunar sample

collections. Consequently, impact-melt breccias remain the most important material used to investigate the impact history of the Moon. Some of these breccias (such as several samples from the Apollo 14 and 15 landing sites) have been linked to Imbrium, based on interpretation of the composition and distribution of Imbrium ejecta using remote sensing observations (e.g., Swann et al., 1971; 1977; Ryder and Spudis, 1987). Other samples have been also considered to be Imbrium ejecta based on geochemical and age similarities to those from the first group. Nevertheless, unlike clast-free impact-melt rocks, lunar impact breccia samples are complex rocks comprising a range of different components from the impact target. These components are commonly shocked and heated to variable degrees. As a result, these samples are extremely inhomogeneous, even on the scale of small hand specimens or thin sections, which can also be reflected in significant variability of ages obtained from different splits of the samples and individual mineral grains. Nevertheless, several decades of painstaking research helped to identify materials that are most likely to homogenize and/or be reset during impacts and therefore provide the most reliable way of dating these events when using different isotope systems, such as U-Pb, $^{40}Ar/^{39}Ar$ and Rb-Sr.

Three types of materials are relevant to the U-Pb system and lunar impact breccia samples:

1. Grains of apatite and merrillite occur in most lithic clasts in breccia samples and as fragments in their matrices. In addition, some of these grains show textural evidence of crystallisation from the impact melt, and therefore directly date impacts. In contrast, fragments of apatite and merrillite and crystals found in the lithic clasts may represent primary magmatic grains within the igneous rocks in the impact target area, and therefore predate impacts responsible for the formation of host breccias. Nevertheless, their U-Pb system can be reset at relatively modest temperature conditions, with the estimated closure temperatures for Pb diffusion on the order of 500 ºC (Cherniak et al., 1991). Consequently, heating associated with the formation of breccia during an impact is, in general, highly likely to drive earlier accumulated Pb out of phosphate grains, resulting in a complete resetting of the U-Pb system, irrespective of the location of these grains either within the clasts or in the matrix (e.g., Thiessen et al., 2018; Snape et al., 2016a). This, however, should not be taken for granted and has to be verified by analysis of multiple grains from the same sample and comparing data from similar samples.

2. Zircon grains commonly represent primary relicts of target rocks and are likely to preserve information related to the formation of these rocks. Taking into account that

the U-Pb system in this mineral is significantly more resistant to thermal pulses than that in phosphates, zircon can also give partially reset ages (Thiessen et al., 2018). However, some lunar breccias are enriched in incompatible elements, most likely due to the presence of high K, P, and REE (KREEP-rich) rocks in the target. Partial melting of this target followed by incorporation of the melt into the breccias and its crystallisation during the cooling of ejecta can result in formation of new zircon grains from the impact melt (Gnos et al., 2004; Liu et al., 2012). These grains are intergrown with the main rock-forming minerals composing the crystallised impact melts and/or contain inclusions of these minerals, indicating their growth from the impact melt, and should yield the age of the impact event. In addition, heating of target material by the impact can result in recrystallization of some previously formed zircon and formation of granular zircon aggregates in the breccia (Cavosie et al., 2015, Timms et al., 2017). Formation of these aggregates is accompanied by complete Pb loss and resetting of the U-Pb system, which can also be used for the dating of impacts (Cavosie et al., 2015, Timms et al., 2017, Kenny et al. 2017; Kenny et al. 2019; Erickson et al., 2020).

3. Clasts of rocks and rock-forming minerals appear to exchange Pb during the impact events and breccia formation. Consequently, Pb is homogenized across the samples, excluding relatively stable zircon grains. This homogenization can also be used to date impacts, constraining Pb-Pb isochrons from the analyses of different phases in breccia samples or individual lithic clasts, providing that zircon is avoided during this analysis (Nemchin et al., 2017; Snape et al., 2017).

Available data based on all three types of materials are presented and discussed in this manuscript. This combination and agreement of data from different constituents of different breccia samples from different landing sites increases confidence in the reliability of obtained ages and indicates that with the exception of one or two potential outliers most of the samples studied using U-Pb system may have originated from a single impact. Considering numerous arguments documented in the literature over the past 50 years and associating different samples from different landing sites to the Imbrium basin, we tentatively interpret these ages as representing the best estimate of the timing of the Imbrium impact.

Filtering of published $^{40}Ar/^{39}Ar$ data obtained for 259 fragments of Apollo breccia samples and updating these data for modern decay constants and monitor ages allows meaningful comparison of U-Pb and $^{40}Ar/^{39}Ar$ ages. This combination permits identification of multiple

192 samples that cannot be viewed as having formed in separate impact events, based on their
193 chronology. Defining this group, which comprises most of the samples from five landing
194 sites, studied using different methods and materials, provides additional means to tackle some
195 of the longstanding questions related to interpretation of samples from different landing sites,
196 such as difference and/or similarity of origin of aphanitic and poikilitic breccias from Apollo
197 17 landing site or explanation for different textural types of Apollo 14 samples. Isolating this
198 key population of samples also helps to identify several breccias with ages that are
199 statistically different from the main group. These samples should be a focus of further
200 chronological studies aiming to confirm their different origin.

201 In general, our approach takes advantage of using ages of the breccias as a preferred
202 parameter to distinguish samples formed by different impacts, as compared to their textural
203 characteristics and chemistry. It follows from the notion that similarity of neither age,
204 chemistry, nor texture of different samples infers their similar origin with a 100% certainty.
205 Differences in chemistry and texture can be attributed to variability of chemical composition
206 of the target and diverse thermal history of the samples during and after the impact and,
207 therefore, are also not completely free of ambiguity. In contrast, difference in ages explicitly
208 implies that two samples are formed by different impacts. All ages, however, are determined
209 with a variable level of analytical uncertainty, which makes the task of assigning samples to a
210 specific age group less than trivial. Consequently, the main aim of this manuscript is to
211 discuss an approach for determination of limits that define the age bracket for a single impact
212 event. This represents a necessary stepping stone for the future discussion of lunar impact
213 history. It is important to note that while the median age and its limits defined in this paper
214 are as robust as currently possible, assigning this age to the Imbrium impact is based on the
215 interpretation of origin of major formations present at the Apollo landing sites, which was
216 developed in the early studies of lunar samples and remote sensing data and still has
217 significant caveats, discussed in this manuscript. Future work based on more recent data
218 (such as those obtained by Lunar Reconnaissance Orbiter, LRO) might result in changes to
219 this interpretation. However, no viable alternative built on this new data sets has been
220 presented to date. Therefore, our interpretation of chronological data follows available
221 interpretations of lunar stratigraphy.

222

223 **2. Analytical techniques and methodology**

2.1. Samples analyzed in this study

This study uses an assembly of different samples represented by basaltic clasts found in the Apollo 14 breccia sample 14305, and phosphate grains from two Apollo 15 breccias (15445 and 15455) as well as rock fragments separated from Apollo 14 soil 14163. This diverse group of samples adds to the range of data that can be interpreted as dating the Imbrium impact. Ability to repeatedly reproduce comparable ages in these texturally different samples supports the argument that their ages represent a profound resetting of the U-Pb system in multiple phases and textural settings by a single impact event.

Sample 14305 was collected about 100 m from the Apollo 14 landing module and is described as a typical breccia representing the Fra Mauro formation exposed at the Apollo 14 landing site and interpreted to represent Imbrium impact ejecta. According to the classification of Simonds et al. (1977) and Stöffler et al. (1980) the sample is a clast-rich, crystalline-matrix breccia. Phosphates in this sample have been analyzed by Snape et al. (2016a). This sample also contains a range of lithic clasts including clasts of Very High Potassium (VHK) basalts that are unique to the Apollo 14 samples (e.g., Ridley, 1975; Shervais et al., 1985b; Neal and Taylor, 1992) and have been analysed as a part of this present study.

Samples 15445 and 15455 were collected from the rim of Spur crater. Both rocks represent a relatively rare example of crystallised impact-melt breccias at the Apollo 15 landing site and both have been interpreted as products of Imbrium ejecta, excavated by Spur (Ryder and Wood, 1977, Ryder and Bower, 1977; Hertogen et al., 1977; Ryder and Spudis, 1987).

Sample 14161 is the 2-4 mm sieved split of bulk soil sample 14163 collected near the Apollo 14 lunar module. Papike et al. (1982) summarized the mineral compositions in 14163 and suggested that the minerals in the soil were mostly derived from the Fra Mauro breccias and/or KREEP basalt. Finkelman (1973) and Devine et al. (1982) studied the finest fractions from this soil and concluded that observed compositional variations could be explained by breaking down of local rocks. Jolliff et al. (1991) showed that rock fragments in sample 14161 represent the large rocks collected at the Apollo 14 site. Consequently, it is likely that the fragments of impact melt investigated here also have a local provenance and possible origin as Imbrium ejecta.

2.2. Sample imaging and identification of targets for U-Pb and Pb-Pb analysis

For samples analyzed at Curtin University, Western Australia, high-resolution optical photomicrographs of the entire thin section of samples were collected using a Zeiss Axio Imager M2m auto-mosaic imaging microscope system (Fig. S1). Targeted regions of interest identified from these images were further characterized using a Tescan MIRA3 field emission scanning electron microscope (FE-SEM) at the Microscopy and Microanalysis Facility, John de Laeter Centre, Curtin University. Backscatter electron (BSE) images and element maps were collected using an Oxford Instruments AZtec combined energy dispersive X-ray (EDX) and electron backscatter diffraction (EBSD) system fitted with an XMax 20 mm Silicon Drift Detector. SEM operating conditions for EDX were 20 kV accelerating voltage, beam intensity of 18, and working distance of 15 mm. The EDX maps were processed for 'TruMap' within the AZtec software, which utilised all X-ray peaks for each element to deconvolve unwanted X-ray counts from overlapping elemental peaks and the removal of X-ray background (which is calibrated specifically for the silicon drift detector for all instrumental settings) to display the real intensity of X-rays for each element (Fig. S2).

For samples analyzed at Washington University, optical context imaging of polished thin or thick sections was done with a Nikon Optiphot Pol petrographic microscope outfitted with a Leica MC170 HD digital camera. Sections were subsequently analyzed with a JEOL JXA-8200 electron probe microanalyzer equipped with 5 wavelength-dispersive X-ray spectrometers with a variety of diffracting crystals. The instrument uses a Gresham E2v silicon-drift energy-dispersive detector capable of X-ray count rates in excess of 200,000 counts/s and with high-speed X-ray mapping and quantitative microanalytical capabilities. Using the electron microprobe, we acquired coregistered secondary-electron, backscattered-electron, cathodoluminescence, and X-ray digital maps at 15.0 kV for context documentation of zircon and phosphate grains using a combination of beam scanning and stage mapping of samples.

2.3. SHRIMP multicollector Pb isotope composition analysis

Pb isotope data for the VHK basalt clasts from Apollo 14 sample 14305 were collected using a SHRIMP IIe MC ion microprobe at the Beijing SHRIMP Center, Institute of Geology, Chinese Academy of Geological Sciences, Beijing. The analyses were calibrated against USGS BCR-2G standard (11 ppm of Pb, Woodhead and Hergt, 2000; Chen et al., 2014) in all analytical sessions.

The mass filtered $^{16}O_2^-$ primary ion beam (with intensity around 2.0 nA) was reduced through a Köhler aperture of 70 µm to obtain a spot size of 10 µm. Before each analysis, an area of 12 µm was pre-sputtered for 120 seconds. This pre-sputtering removed the gold coating from the area around the analytical spot and further limited the effects of surficial sample contamination. This procedure was followed by automatic centering of the secondary ion beam in the 80 µm source slit and automatic centering of the magnetic field. The secondary ions were measured using a static mode with four low-noise channel detection electron multipliers (CDEM). Detector gains were measured before each session by stepping ^{206}Pb through all collectors. Differences in detectors' gains, however, were also monitored and corrected using multiple runs of the BCR-2G standard during each session, dispersed between analyses of unknowns. Baseline measurements were also performed at the beginning of each session.

Following the SHRIMP analyses, SEM images of the analyzed spots were acquired in order to determine their exact location and identify any outliers related to fractures or grain boundaries. These analyses were excluded from the final dataset.

Reduction of the SHRIMP data was done manually in Excel. Final ages and plots were made using the Isoplot Excel add-in (version 4.15; Ludwig, 2008). All analytical data are reported at 1σ, whereas final ages are presented at the 95% confidence level (unless specified).

2.4. SHRIMP U-Pb analysis of phosphates and zircon

U-Pb isotopic data for phosphates and zircon from Apollo 14 samples were collected using a SHRIMP II ion microprobe at the Beijing SHRIMP Center, Institute of Geology, Chinese Academy of Geological Sciences, Beijing. Sample mounts for SHRIMP analysis were coated with gold and U–Pb measurements were done following established operating procedures described by Williams (1998). The U/Pb ratios in phosphates were calibrated against the 2058 Ma apatite crystal BRA-1 (67 ppm of U and $^{206}Pb/^{204}Pb$ of 500, Grange et al., 2009) in all analytical sessions. Zircon data were calibrated against Ceylon zircon BR266 (Stern et al., 2001).

The mass filtered $^{16}O_2^-$ primary ion beam (with intensity around 1 nA) was reduced through Köhler apertures of 50 µm to obtain spot size of 8 µm. Before each phosphate and zircon analysis, an area of 12 µm was pre-sputtered for 300 seconds. This procedure was followed by automatic centering of the secondary ion beam in the 80 µm source slit and automatic centering of the magnetic field. Secondary ions were measured using a peak-hopping routine

with a single low-noise electron multiplier. The mass spectrometer was operated with a mass resolution of 5600 (M/ΔM), sufficient to separate Pb peaks from molecular interferences.

Reduction of the SHRIMP data was done using SQUID and Isoplot add-ins (version 4.15; Ludwig, 2008). All analytical data are reported at 1σ, whereas ages of the samples are presented at the 95% confidence level (unless specified).

2.5. Cameca IMS 1280 U-Pb analysis of phosphates

U-Pb isotopic data for phosphates from the Apollo 15 (15445 and 15455) samples were collected using a CAMECA IMS 1280 ion microprobe at the NordSIMS facility, Swedish Museum of Natural History, Stockholm. The SIMS methodology closely followed the analytical description published elsewhere (Nemchin et al., 2009; Snape et al., 2016a). The U/Pb ratios in phosphates were calibrated against the 1160 Ma apatite crystal NW-1 (Li et al., 2012) in all analytical sessions, while the differences in detectors' gains were monitored and corrected using multiple runs of the BCR-2G standard (Woodhead and Hergt, 2000).

The mass filtered $^{16}O_2^-$ primary ion beam (with intensity around 0.7 nA) was reduced through Köhler apertures of 50 µm to obtain a spot size of 5 µm. Before each phosphate analysis, an area of 12 µm was pre-sputtered for 80 seconds to remove the gold coating from the area around the analytical spot and further limit the effects of surficial sample contamination. This procedure was followed by automatic centering of the secondary ion beam in the 4000 µm field aperture and automatic centering of the magnetic field. The secondary ions were measured using 4 low-noise (<0.01 counts per second) ion counting electron multipliers (Hamamatsu 4146) with electronically-gated deadtimes of 65 ns. Background counts for each channel were measured at regular intervals during each session, and individual analyses were filtered out of the final dataset if the count rates for any masses were lower than 3× the background count rates during that session. The four Pb isotopes were measured in separate electron multipliers, one of which was also used to measure secondary ion beam intensities in a mass-switching sequence that included $^{40}Ca^{31}P^{16}O_4^+$ (the matrix peak for the phosphate measurements), $^{238}U^+$, $^{232}Th^{16}O^+$ and $^{238}U^{16}O^+$. The mass spectrometer was operated with a mass resolution of 4860 (M/ΔM), sufficient to separate Pb peaks from molecular interferences.

Following the SIMS analyses, SEM images of the analyzed phosphate grains were acquired to determine the exact location of SIMS spots and to identify any likely sources of error in

the measurements (e.g., whether the SIMS spots hit fractures or grain boundaries). Analyses which clearly hit fractures or grain boundaries were excluded from the final dataset.

Reduction of the SIMS data was done using in-house software developed at NordSIMS for the CAMECA 1280 analyses and the Excel add-in Isoplot (version 4.15; Ludwig, 2008) was used to calculate ages. All analytical data are reported at 1σ, whereas ages of the samples are presented at the 95% confidence level (unless specified).

2.6. Comparison of SHRIMP and Cameca IMS 1280 analytical results

Analytical protocols for investigation of U-Pb systems in U-bearing minerals such as zircon and apatite are very well established and tested during several decades of extensive work using both SHRIMP and IMS 1280 (1270) instruments around the world. However, it is the first time when SHRIMP muticollector system was used to obtain Pb isotope compositions for the low Pb minerals in lunar samples. As the analytical procedure involves periodic analysis of a standard (BCR-2G) in order to correct data for detectors' gain, these standard analyses can be used to compare performance of two instruments used in this study. Table-1 presents BCR-2G data obtained during two separate sessions run using SHRIMP in Beijing and two sessions from IMS 1280 in Stockholm. The data indicate that both external and internal reproducibility for all Pb isotope ratios is about two times worse for the SHRIMP multicollector. Both levels of uncertainties, however, make insignificant contributions (less than few percent) to the final estimates for uncertainties of ratios in lunar samples. Slight differences in the values between different sessions and instruments are a result of different detector gains, and are used to correct analyses obtained for lunar samples, by normalizing to the published BCR-2G values (Woodhead and Hergt, 2000).

2.7. Correction of phosphate and zircon data for initial lunar Pb and terrestrial (laboratory) contamination

Proper correction for Pb that is incorporated in a mineral during its formation (or impacts that modified its isotope system), rather than in-situ accumulation from U decay after the formation (or impact), is especially critical in lunar U-Pb chronology as Pb is generally depleted in the Moon. This depletion results in high U/Pb ratios in lunar silicate reservoirs and, consequently, very radiogenic Pb isotope compositions. As such, initial lunar Pb can have an isotope composition barely distinguishable from that of in situ accumulated Pb, which can result in overestimation of ages. The issue is complicated even further by the ubiquitous presence of terrestrial Pb in all samples, which in case of Apollo samples is

381 introduced during sample preparation and handling, even though the most extreme care is
382 taken by the Astromaterials Curation Group at Johnson Space Centre (JSC) in Houston to
383 avoid any contamination during sample handling and thin section preparation. For samples
384 that have been allocated previously, some of the potential contamination could be introduced
385 during research conducted in multiple labs outside of JSC. In lunar meteorites, contamination
386 can also result from the prolonged residence of the samples at the surface of the Earth.

387 The expected combined presence of initial lunar Pb and contamination generally undermines
388 the ability to make an accurate correction in order to determine true in-situ Pb compositions
389 and extract ages of the samples with a high degree of confidence. Some assumptions are
390 made to combat the problem. In general, when U-bearing minerals such as zircon and
391 phosphates are analyzed, the assumption is that these phases did not incorporate lunar initial
392 Pb when they formed and all extra Pb, which is not associated with the in situ U decay,
393 comes from contamination. A modern model terrestrial Pb composition (Stacey and Kramers,
394 1975) is then applied for correction (e.g., Nemchin et al., 2008, and all following publications
395 from different laboratories around the world). This assumption, however, is not entirely
396 correct even for zircon, which usually excludes Pb during crystallization.

397 For samples modified by impacts, it is commonly assumed that all Pb was driven out of the
398 analytical target by the impact, so that there is no Pb, accumulated in the minerals prior to the
399 impact, left in the analyzed volume. The uncertainty associated with this assumption is
400 illustrated by examination of previously published data. Some results of phosphate dating for
401 Apollo 12 and 14 samples discussed in detail by Thiessen et al. (2018) and Snape et al.
402 (2016a) are presented in Figure 1 using one of the sets of coordinates described by Tera and
403 Wasserburg (1973). The choice of this particular coordinate system is determined as a matter
404 of convenience, as both lunar initial and terrestrial Pb are plotted at the lower-left part of the
405 $^{206}Pb/^{207}Pb$ vs. $^{238}U/^{207}Pb$ diagram, resulting in less stretching along the vertical axis. The
406 lunar initial composition in this study was selected to correspond to the value determined by
407 Nemchin et al. (2017) to be an average composition of Apollo 14 breccias (Fra Mauro
408 formation) at 3.9 Ga. This composition is viewed as most appropriate given that the majority
409 of samples discussed here were collected at the Apollo 14 site. While the selected Pb
410 composition may not be equally representative of the other landing sites, there are no similar
411 estimates made for these sites with a possible exception of the Apollo 16 composition
412 proposed by Snape et al. (2017) and shown in Figure 1a. Taking into account that Apollo 14
413 breccias are among the most U-rich samples available in the lunar collection, whereas Apollo

16 samples are among those with the lowest U content, the possible range of initial lunar Pb isotope compositions in the investigated samples should not have a significant effect on the resulting age estimates.

The modern composition of terrestrial Pb estimated from the Stacey and Kramers (1975) model was used to correct Pb data in the original work of Thiessen et al. (2018) and Snape et al. (2016a). For phosphates in the Apollo 12 sample 12013 (Fig.1a, b, and c), this selection appears to be valid as the analytical points fall on a single line in $^{206}Pb/^{207}Pb$ vs. $^{204}Pb/^{207}Pb$ coordinates, projecting back to the Stacey and Kramers (1975) composition. A steep trajectory of this correction in 3D $^{206}Pb/^{207}Pb$-$^{204}Pb/^{207}Pb$-$^{238}U/^{207}Pb$ space leads to a relatively small shift of analytical points in the $^{206}Pb/^{207}Pb$-$^{238}U/^{207}Pb$ plane as a result of this correction (comparison between Fig.1b and c). If a lunar initial Pb composition is applied to this data set, the much shallower trajectory of this correction (Fig.1a and b) would make all ages significantly younger and spread the points over a range of several hundred million years on the concordia diagram, with some points projecting away from the concordia curve.

Data for the sample 14305 (Fig.1d, e, and f) show a similar linear trend in $^{206}Pb/^{207}Pb$ vs $^{204}Pb/^{207}Pb$ coordinates. However, the best fit appears to project away from the pure Stacey and Kramers (1975) composition and intersects a mixing line between this composition and lunar Pb (Fig.1d). In fact, terrestrial Pb appears to be just outside of the error envelope constrained for this line. Consequently, it is feasible to consider a small contribution of lunar initial Pb in the total Pb present in phosphates analyzed in this sample, and the best composition for correction is therefore defined by the intersection of the best fit line through analytical points and the mixing line between terrestrial and lunar initial compositions. Such correction results in narrowing the spread of the analytical points on the concordia diagram (Fig.1e and f).

Samples 12013 and 14305 present relatively simple relationships where all analyses fall on a line in plots of $^{206}Pb/^{207}Pb$-$^{204}Pb/^{207}Pb$, suggesting that measured Pb of all analyses in these samples can be corrected using a single composition representing similar proportions of lunar initial Pb and contamination. However, this is not always the case. The majority of phosphate analyses in sample 14314 (Fig.1g, h and i) show a similar simple relationship, falling on a line (Fig. 1g) that intersects the mixing line between lunar initial composition and contamination at approximately the same distance from the end components as that observed for the breccia 14305. The error envelope is larger owing to the much smaller spread of analyses in sample 14314. Nevertheless, using the Pb composition defined by the intercept of

two lines can potentially make all ages younger than those obtained when a pure Stacey and Kramers (1975) composition is applied for the correction. Regardless, the main additional complication in this data set is that four analyses of one phosphate grain appear to fall outside the line defined by other analyses (Fig.1g). Correcting these analyses using either the Stacey and Kramers (1975) model composition or that defined from the best fit line results in the older ages for this single grain (Fig.1h and i). This result led to the conclusion by Snape et al. (2016a) that this grain was potentially incorporated into breccia 14314, interpreted to be a part of Imbrium ejecta, as a result of mixing of this ejecta with some older underlying units, rather than being from a single target rock population. However, it is also possible that this grain contains a larger proportion of lunar initial Pb. This possibility would result in much steeper correction trajectory, which would bring these analyses in line with the rest of the phosphate data obtained for this sample. Choosing between two possible interpretations is impossible based on Pb isotope data alone.

In theory, the problem of choosing between multiple interpretations can be alleviated by adding U/Pb to the Pb isotope systematics and recognizing that a plane drawn through lunar initial Pb, terrestrial contamination, and an analytical point in 3D coordinates, such as $^{206}Pb/^{207}Pb$-$^{204}Pb/^{207}Pb$-$^{238}U/^{207}Pb$, will cross the concordia curve at the time corresponding to formation of the sample. If the sample was affected by a later event and the analysis is discordant, the plane will intersect the concordia at two points, i.e., aligning on a discordia with two concordia intercepts that represent the time of crystallization and subsequent disturbance. This approach would allow separate calculations to be made for individual analyses, eliminating the need to constrain lines using multiple analytical points, which inadvertently involves making the assumption that all these analytical points represent similar materials with the same age and origin. The use of U/Pb is, however, limited by the need to correct measured elemental ratios such as U/Pb for the matrix-related ionization efficiency differences between different elements. As a consequence, the best analytical error for U/Pb that can be achieved by currently available SIMS methods is in the range of 1-2%, which can translate into an error of several hundred million years in the calculated ages for lunar materials. This is because the Pb correction trajectories are almost parallel to the concordia curve in the time interval most relevant to the Apollo breccias (e.g., Fig.1b, e, and h). In addition, a significant number of U-Pb analyses of lunar zircon and phosphates by SIMS appear to be slightly reversely discordant, probably also due to imperfect correction for the matrix effects when target grains (commonly analyzed within a thin section) and reference

standards (in epoxy mounts) have different surface polish qualities and are analyzed separately (e.g., Nemchin et al., 2008).

The currently existing difficulty in applying the full U-Pb systematics to the correction of analytical data for the influence of mixed contamination and lunar initial Pb means that constraining lines in $^{207}Pb/^{206}Pb$-$^{204}Pb/^{206}Pb$ (or $^{206}Pb/^{207}Pb$-$^{204}Pb/^{207}Pb$ as presented here) coordinates is the best available approach. This approach allows the proportion of two components in the mixture to be determined and possible outliers to be identified. Interpretation of these outliers remains controversial. Nevertheless, their presence in some samples makes age determinations based on a small number of analyses unreliable. Using corrections based simply on the assumption of terrestrial contamination with no presence of initial lunar Pb can generate systematic errors and appears to be inferior to the lines regressed through the data points. The ages can be determined directly from the lines, but it is also important to verify that a regression line projects between terrestrial and lunar initial Pb compositions, rather than passing outside of the limits defined by these compositions, which may indicate mixed age populations. This line-fitting approach has been adopted in the present study for all new analyses. Previously published data have been also recalculated using this approach.

2.8. Filtering and updating $^{40}Ar/^{39}Ar$ data

In order to compare previously published $^{40}Ar/^{39}Ar$ results and U-Pb ages, the $^{40}Ar/^{39}Ar$ data sets need to be recalculated using recently updated decay constants and monitor ages, which themselves were calibrated against U-Pb ages (Renne et al., 2011). We have evaluated only analyses obtained for the fractions of impact melt with ages obtained by the $^{40}Ar/^{39}Ar$ step-heating technique because they appear to be easiest to interpret, at least when a relatively simple plateaus are formed by sequential Ar release steps. This, however, also requires to establish set of parameters that can be used to define a plateau. The adopted approach comprised:

1. Accepting only data where the calculated weighted-mean ages combine at least 3 consecutive steps either including between 50% and 70% of degassed ^{39}Ar (producing a ‘mini-plateau’, i.e. somewhat acceptable but in need of independent corroboration by a robust age) or comprising more than 70% (producing a plateau, i.e. can be considered robust) of ^{39}Ar degassed (e.g., McDougal & Harrison, 1999 and references therein; Jourdan, 2012; Kennedy et al., 2013);

2. Accepting only plateau (and mini-plateau) ages with a probability of fit (P) ≥ 0.05 as statistically valid (e.g., Mahon, 1996; Baksi, 2007a; Jourdan et al., 2009).

These statistical tests permit evaluation of the internal homogeneity of the analysed samples, which is of particular significance given that most of the breccias contain small clasts of different origins that are not always easy to distinguish from the matrices. The criteria allow the selection of samples with a simple history and with no subsequent perturbations of the K-Ar system. The MSWD and P values reflect the goodness of fit and verify that the scatter within a group of measurements (e.g., the steps defining an apparent plateau) can be explained by the uncertainties of the measurements alone and thus, belong to a single population (e.g., Mahon, 1996; Baksi, 2007b; Jourdan et al., 2009).

In addition to the filtering, all data have been normalised to common standard (Hb3gr, NL-25-2, MMhb-1) ages to enable comparison between different data sets as well as for updated decay constants in order to compare to other isotope systems (Renne et al., 2011). The J-value is a proxy for the neutron irradiation efficiency that allows the creation of ^{39}Ar from ^{39}K and is therefore a source of analytical error. As the J-value and its error vary from sample to sample, the uncertainty on the J-value must be propagated in the final age calculation so that $^{40}Ar/^{39}Ar$ ages obtained using different irradiation parameters can be compared. However, much of the published $^{40}Ar/^{39}Ar$ ages do not account for the errors in J-value. In addition, $^{40}Ar/^{39}Ar$ dates rarely include systematic errors such as the error on the age of the monitor (used to calculate the J-value) and the error on the ^{40}K decay constant (λ). The latter becomes important when comparing $^{40}Ar/^{39}Ar$ ages to those obtained using other isotope systems. Published results that do not (i) provide information about the standard (type and age) used and/or (ii) where a complete set of data cannot be tested against criteria described above were excluded from the comparison. The former is especially important considering that the ages of standards adopted at the time of the publications are often updated by recent studies.

Taking all these potential sources of uncertainty into account, data have been replotted using Isoplot (Ludwig, 2003) in order to identify data sets that form plateaus and mini-plateaus. All $^{40}Ar/^{39}Ar$ plateau and mini-plateau ages published prior to 1977 were also recalculated using the decay constants recommended by Steiger and Jäger (1977) and associated standard ages of 1074 ± 5 Ma for Hb3gr (Jourdan et al., 2006), 2660 ± 9 Ma for the hornblende standard NL-25-2 recalculated by Schwarz and Trieloff (2007) and 523.1 ± 2.6 Ma for the MMhb-1 hornblende standard. Furthermore, all ages have been subsequently recalculated using the more recent decay constants and associated standard ages (e.g., Hb3gr = 1081 ± 1.2 Ma)

recommended by Renne et al. (2011), which are fully calibrated against the U-Pb system (Table 6).

2.9. Updating Rb-Sr data

A small group of published Rb-Sr data obtained from the samples that can be interpreted as representing impact melts has been reprocessed using Isoplot (version 4.15; Ludwig, 2008) to ensure consistency between the ages. In addition, Rb decay constant of 1.402×10^{-11} a^{-1} suggested originally by Minster et al. (1982) was used in all calculations. These authors suggested a change in decay constant in order to account for the differences in Rb-Sr and U-Pb systematics of chondrites. Consequently, their value can provide better grounds for similar comparison in this current manuscript.

3. Results

3.1. Basaltic clasts in Apollo 14 breccia thin section 14305,103

The petrographic section of sample 14305 investigated here contains several clasts of very fine-grained breccia ranging in size from 1-2 mm to almost a centimeter, surrounded by matrix consisting mostly of smaller fragments (10 to 100 μm across) of similar material, predominantly pyroxene and plagioclase with a smaller amount of opaques (Figure S1). Five clasts of subophitic basalt have also been identified in the section (Figure S1). EDS mapping of the clasts indicates a VHK (Very High Potassium) composition of the clasts (Figure S2). K-feldspar is developed as an interstitial phase throughout the clasts between the laths of plagioclase and Ca-rich pyroxene. Abundant elongated ilmenite crystals are intergrown with the interstitial K-feldspar.

The K-rich areas within the clasts have been targeted during SHRIMP analysis of Pb isotope compositions. Pb was analyzed in a total of 114 spots (20 μm across) within the basaltic clasts Table 2). The large number of analyses was dictated by the exceptionally high level of contamination by terrestrial Pb, unusual even for the Apollo 14 breccia samples, which are found to be more contaminated than similar samples from other landing sites. This resulted in the need for a larger number of analyses to identify those that contain exclusively lunar Pb. The approach follows a previously developed assumption (Snape et al., 2016b; 2017; Nemchin et al., 2017) that the majority of lunar samples contain Pb representing a simple three component mixture: (i) in situ accumulated Pb, formed as a result of U decay after the latest closure of the U-Pb system in the sample; (ii) lunar initial Pb, accumulated in the

577 sample prior to the latest closure of the U-Pb system or added to the sample during its
578 formation, and (iii) terrestrial contamination that can be attributed to the history of a sample's
579 processing (e.g., cutting of thin sections) and previous analytical work in different
580 laboratories, including our own studies. This third component appears to be particularly
581 ubiquitous in the sections of Apollo 14 breccias, possibly due to their relatively high porosity
582 and abundance of fractures. These physical properties of the samples make removal of
583 contamination virtually impossible even when standard surface cleaning procedures
584 commonly used for ion probe sample preparation are applied.

585 The analyzed section appears to represent an excellent example of this three component
586 mixture (Fig. 2a), which is expected to result in all analytical points falling within a triangle
587 with apices defined by three components on the $^{207}Pb/^{206}Pb$ vs. $^{204}Pb/^{206}Pb$ diagram. The large
588 number of analyses obtained for the section 14305,103 allows a statistically robust definition
589 of all sides and apices of the triangle, even though a number of analyses plot within the
590 triangle. The leftmost steepest side of the triangle (Fig. 2a) represents lunar Pb that is free of
591 contamination (i.e., a Pb-Pb isochron defining the closure time of the U-Pb system in the
592 analyzed phases). The intercept of this isochron and the vertical axis defines the age for the
593 last homogenization event experienced by the sample as 3927±35 Ma (95% confidence). A
594 similar age of 3933±10 Ma (95% confidence) can be determined from the analyses falling on
595 the lower side of the triangle (Fig. 2a); these analysis spots are assumed to be free of lunar
596 initial Pb and form a line that we interpret as mixing of terrestrial Pb (component-3 in the
597 above description) and in-situ accumulated Pb (component-1). The top side of the triangle
598 contains analyses representing a mixture of initial lunar Pb (component-2) and terrestrial
599 contamination. Intersection of this line with the lunar Pb line (steepest, leftmost side of the
600 triangle) gives the best estimate of Pb composition in the sample during its last closure at
601 approximately 3.93 Ga (i.e., lunar initial Pb). The $^{207}Pb/^{206}Pb$ and $^{204}Pb/^{206}Pb$ for this Pb are
602 1.350±0.023 and 0.00248±0.00014.

603 The constraints and the assumption of a three component mixture for the analyzed sample is
604 further supported by the behavior of data points in the $^{208}Pb/^{206}Pb$ vs. $^{204}Pb/^{206}Pb$ diagram
605 (Fig. 2b). In general, the analyses representing lunar Pb free of contamination are not
606 expected to form a line in these coordinates, because $^{208}Pb/^{206}Pb$ in any particular sample
607 depends on the variability of Th/U in different phases targeted by the analytical spots, in
608 addition to the age of the sample. Nevertheless, in 14305,103 data form a linear trend at the
609 leftmost side of the data array. On the other hand, analyses representing a pure mixture of

initial lunar Pb and contamination must fall on a line, assuming a similar initial lunar Pb isotope composition in all minerals in the sample and also similarity of the composition for terrestrial contamination. This expectation is supported by data where (with an exception of one analysis) all data points representing mixing between initial Pb and contamination identified from $^{207}Pb/^{206}Pb$ vs. $^{204}Pb/^{206}Pb$ also plot on a line in the $^{208}Pb/^{206}Pb$ vs. $^{204}Pb/^{206}Pb$ coordinates. The $^{208}Pb/^{206}Pb$ of the lunar initial Pb is determined to be 0.881±0.056, from the equation of this line and using a $^{204}Pb/^{206}Pb$ value of 0.00248±0.00014 determined from $^{207}Pb/^{206}Pb$ vs. $^{204}Pb/^{206}Pb$. None of the analytical points are allowed to fall below the line constrained from the origin of the $^{208}Pb/^{206}Pb$ vs. $^{204}Pb/^{206}Pb$ diagram and passing through the composition of terrestrial contamination, as this would indicate a negative $^{208}Pb/^{206}Pb$ corresponding to this analysis. This limit generally holds for all analyses of 14305,103, with exception of a single analytical spot, which also has the largest analytical errors in the data set and is probably an analytical artefact.

3.2. Phosphates from Apollo 15 breccia thin sections 15445,62 and 15455,30

The thin sections investigated in this study are typical examples of the two parent samples (15445 and 15455). Section 15445,62 (Figure S3) shows interfingering areas of fine-grained (5-20 μm grain size) matrix and brecciated lithic clasts similar to that described by McGee et al. (1979). Section 15455,30 contains fragmented breccia crosscut by the impact-breccia matrix in the middle of the thin section (Figure S4). Four apatite grains have been identified in section 15445,62, and three appear to be attached to larger mineral fragments. Eight additional phosphate grains were analysed within the brecciated lithic part of section 15455,30.

The majority of SIMS analyses show $^{206}Pb/^{204}Pb$ ranging between a few hundred to a few thousand (Table 3). However, there are two analyses with $^{206}Pb/^{204}Pb$ in excess of 10,000, which makes them relatively insensitive to the choice of initial or contamination Pb correction. In addition, all data uncorrected for contribution of either lunar initial or terrestrial contamination Pb plot on a single line in $^{207}Pb/^{206}Pb$ vs. $^{204}Pb/^{206}Pb$ coordinates (Fig.3a) indicating a similar proportion of these two components (but dominated by the contamination) incorporated by all analysed apatite grains. Consequently, all analyses have been corrected for a single, similar composition of excess Pb, which does not originate from in situ U decay. This composition was determined by the intersection of the best fit line derived from the analytical points and the line joining the modern terrestrial Pb composition determined from the Stacey and Kramers (1975) model and model lunar Pb at 3.9 Ga

(Nemchin et al., 2017). Corrected analyses plot slightly to the left of the Tera-Wasserburg concordia curve (Fig. 3b), most likely as a result of the influence of matrix effects not fully accounted for by the analysis of the standard apatite sample. Nevertheless, corrected $^{207}Pb/^{206}Pb$ values (not influenced by instrumental matrix effects) define a weighted mean age of 3915±6 Ma (Fig. 3c, MSWD = 0.62 and a probability of 0.92), which is interpreted as the best estimate for the age of the investigated phosphate grains and the time of the formation of breccias 15445 and 15455.

3.3. Phosphates in fragments from 14161

14161,7125 is a 3 mm fragment of an impact-melt breccia (Jolliff et al., 1991; Figure S5). It consists of a mixture of mineral clasts (pyroxene and plagioclase) ranging in size from 0.5 to about 0.1 mm, gradually transitioning into the matrix of similar mineral composition with the interlocking 5 to 20 μm pyroxene and plagioclase grains. The matrix also hosts numerous zircon, merrillite, and apatite grains of similar size. Some of the zircon grains may represent fragments inherited from the rocks melted during the formation of the sample, similar to large clasts of pyroxene and plagioclase. For example, of eight analysed zircon grains, zircon-1 and zircon-6 appear to have, at least in part, morphologies that are distinct from the surrounding mineral assemblage (Fig. 4). However, one side of zircon-1 forms embayments similar to those present in the surrounding minerals. Consequently, it is equally possible that this grain formed as an integral part of impact melt crystallization or has been partially resorbed by the melt. Less ambiguous signs of growth within the melt are shown by the embayed edges and poikilitic texture of grain-7, consistent with the surrounding pyroxene and plagioclase grains. Other investigated grains could be interpreted as partly resorbed fragments of pre-existing zircon or as having grown directly from the melt. Nevertheless, the presence of small (a few μm long) zircon grains throughout the section that are euhedral to subhedral and appear to be an integral part of the mineral assemblage in the matrix, strongly suggests that zircon growth took place during impact-melt crystallization. This could have happened either directly from Zr-saturated melt when it cooled, or by partial dissolution of pre-existing zircon fragments and crystallization of multiple small grains. In contrast, some apatite grains appear to be more angular (broken) and may represent fragmented crystals that have been incorporated into the melt from its source, especially in the case of apatite-1, which is much larger than the surrounding matrix (at about 100 μm across) and angular (Fig.4).

U-Pb analyses of seven zircon grains (Table 4) in this sample show a typical Apollo 14 age distribution pattern with three grains having ages around 4.3-4.2 Ga, three at about 4.0 Ga,

676 and one at about 4.1 Ga (Fig. 5a). However, six analyses of three apatite grains indicate
677 significantly younger ages. All but one SIMS analysis have $^{206}Pb/^{204}Pb$ in excess of 10,000
678 (Table 4), which makes the difference between the uncorrected $^{207}Pb/^{206}Pb$ and $^{238}U/^{206}Pb$
679 ratios and those corrected for either initial lunar Pb or terrestrial contamination negligible
680 within the analytical uncertainties. One analysis with a slightly lower $^{206}Pb/^{204}Pb$ of about
681 5000 makes it possible to fit a relatively imprecise line through the analytical points in
682 $^{207}Pb/^{206}Pb$ vs. $^{204}Pb/^{206}Pb$ coordinates (Fig. 6a, b), which was used to correct the data for ex
683 situ Pb components. This line appears to indicate a slightly larger contribution of lunar initial
684 Pb relative to terrestrial contamination in this group of apatite grains, compared to those
685 found in the investigated Apollo 15 sections (Fig. 3a). The corrected data plot to the left of
686 the Tera-Wasserburg concordia curve (Fig. 6c), similar to the Apollo 15 apatite grains, and
687 yield a weighted average $^{207}Pb/^{206}Pb$ age of 3917±14 Ma (Fig. 6d, MSWD= 1.4, probability
688 of 0.22).

689 Impact melt rock 14161,7233 has a fine-grained, intersertal texture and abundant minor and
690 accessory minerals including ilmenite, zircon, merrillite, and apatite, typically with grain
691 sizes of 5-50 μm, but with several domains of coarser and finer grain sizes. Plagioclase
692 occurs as elongate lath-shaped grains up to 0.4 mm in length and with intersertal pyroxene of
693 grain sizes up to 0.2 mm in size (Figure S6, Jolliff et al., 1991; Jolliff, 1998). On the basis of
694 mineral compositions, the section contains no obvious xenoclasts. Zircon appears to form an
695 integral part of the finely crystalline texture showing regular intergrowths with the major
696 minerals, sizes from about ~2 to 30 μm and euhedral to subhedral crystal shapes (Fig. 7a).
697 Some zircon grains (Fig. 7b) also show granular textures characteristic of impact-related
698 recrystallization (Wittmann et al., 2006; Cavosie et al., 2016; Timms et al., 2017). Sixteen of
699 seventeen analyses of 11 grains show ages around 4.31 Ga. One grain indicates a younger age
700 around 3.96 Ga (Fig. 5b). Apatite and merrillite in the fragment also show textural
701 relationships indicating their crystallization with the major minerals (Fig. 7c and d). Merrillite
702 commonly occurs adjacent to and contacting ilmenite grains of the same size. Some apatite
703 grains are as elongated as those of pyroxene and plagioclase and reach lengths of 100-200 μm
704 (e.g., Apt 1, Fig. 7C.

705 Seven SIMS analyses of six apatite and six analyses of six merrillite grains (Table 4) indicate
706 complexity not visible in the apatite analysed in sample 14161,7125. Importantly $^{206}Pb/^{204}Pb$
707 in the investigated grains vary from about 350 to 4500, which makes these analyses sensitive
708 to the choice of Pb isotope composition to correct for the contribution of lunar initial Pb and

709 contamination. In addition, analyses do not form a single linear trend in $^{207}Pb/^{206}Pb$ vs.
710 $^{204}Pb/^{206}Pb$ coordinates (Fig. 8a), in contrast to the Apollo 15 sample and fragment
711 14161,7125. The lack of a linear trend indicates either that the grains have a different age (if
712 a single Pb composition is applied for correction) or that the proportion of lunar initial and
713 contamination varies from one analysis to another (in which case all analyses can be forced to
714 fit a single age, which would also define different proportions of lunar initial Pb and
715 contamination). A line can be fitted through six (three apatite and three merrillite) analyses
716 with the lowest $^{207}Pb/^{206}Pb$ (Fig. 8a), which defines a Pb isotope composition for correction,
717 similar within the uncertainties to that determined from fragment 14161,7125 data. If a
718 composition significantly more enriched in the lunar component is used for the correction, it
719 would result in significantly (perhaps unrealistically) younger ages obtained from these six
720 analyses. The observed complexity of the data reduces the reliability of the U-Pb age
721 obtained for this rock fragment. In the best case scenario, six analyses (most of which also
722 have highest $^{206}Pb/^{204}Pb$) can be considered to represent a true age when the phosphate U-Pb
723 system was locked for any further Pb mobilization, defined by a weighted mean of 3922±24
724 Ma (Fig. 8c, MSWD= 1.4, probability of 0.21). In the worst case, this age defines an upper
725 limit for the closure of U-Pb systems in phosphates from the fragment 14161,7233.

726 Impact melt fragment 14161,7060 is a clast-bearing impact-melt breccia (Jolliff et al., 1991),
727 more similar to 14161,7125 than 14161,7233 in that it contains large (up to 0.5 mm across)
728 clasts of plagioclase and pyroxene surrounded by a fine-grained pyroxene-plagioclase matrix
729 (Figure S7). Zircon and phosphates are abundant in the matrix but most grains are << 10 μm
730 in size. About a dozen zircon and merrillite grains occur in the 10-20 μm grain size and were
731 targeted during SHRIMP analysis.

732 Two zircon grains show indistinguishable ages around 4.31 Ga, whereas one is significantly
733 younger at about 4.03 Ga (Fig.5c, Table 4). Four analyses of three merrillite grains have
734 $^{204}Pb/^{206}Pb$ ranging from about 1200 to 4500, but define a line in $^{207}Pb/^{206}Pb$ vs. $^{204}Pb/^{206}Pb$
735 coordinates (Fig. 9a) passing directly through the modern terrestrial Pb composition.
736 Correcting for this Pb, results in a slightly discordant $^{207}Pb/^{206}Pb$ vs. $^{238}U/^{206}Pb$ ages
737 (analytical points fall to the right of the Tera-Wasserburg Concordia curve in Fig. 9b).
738 However, a weighted average $^{207}Pb/^{206}Pb$ age of 3924±27 Ma (MSWD= 0.03, probability of
739 0.99; Fig. 9c) is indistinguishable, within analytical uncertainty, from the ages obtained for
740 the phosphates from the two other fragments (14161,7125 and 14161,7233).

741

4. Discussion

4.1. Pb-Pb ages of lithic clasts and matrices in the impact melt breccias

Initial attempts to investigate individual lithic clasts in the impact breccia samples using the Pb-Pb isotope system were aimed at determination of ages of the rocks represented by these clasts (e.g., Nemchin et al., 2017). It has become evident, however, that Pb is profoundly homogenized across the clasts and even breccia samples during the impacts that assembled the samples. Therefore, Pb-Pb isochrons obtained during these studies define ages of the breccias, and hence date impact events. In addition to five VHK basalt clasts from the sample 14305 analyzed here, the currently available data set (Table 5) comprises two felsic clasts in sample 14083 and one "granite" clast in sample 14303 (Nemchin et al., 2017). Furthermore, Snape et al. (2017) investigated a large range of mineral phases in the Apollo 16 breccia sample 66095. The similarity of ages obtained independently for two millimeter-size clasts in sample 14083 (Nemchin et al., 2017) supports the assumption of complete homogenization of Pb isotopes on the sample scale. Equally, the similarity of the ages obtained from the clasts in three different Apollo 14 samples (14303, 14305, and 14083) suggests that these breccias formed in the same event.

The interpretation of the origin of the sample 66095 is complicated by its original location on the Moon. It was chipped off a 0.5 m boulder on the rim of a 10 m crater at Station 6. This was one of the southernmost points of the Apollo 16 traverse, located close to the boundary between the Cayley Plains and Descartes Mountains units, at the foot of Stone Mountain (the southern outcrop of the Descartes unit). These two units have been correlated with different impacts in various, and in some cases conflicting, ways (Head, 1974; Spudis, 1998; Haskin et al., 2003; Norman et al., 2010; Joy et al., 2011). A common view is that the Cayley Plains unit is ejecta resulting from the Imbrium basin-forming event and was deposited ballistically on the older Descartes material, which was introduced to the region by an earlier impact event, such as the formation of the Nectaris basin (e.g., Head, 1974). An alternative interpretation proposes that two units represent different ejecta facies from the same (Imbrium) basin (e.g., Muehlberger et al., 1980; Norman et al., 2010). Both views appear to be in agreement regarding the Imbrium origin of the Cayley Plains unit.

Regardless of the interpretation of 66095, the similarity of the Pb-Pb age of this sample and three Apollo 14 samples indicate that they all could have been formed in the same impact

773 basin or at least by two contemporaneous impacts. Combining all five age estimates gives a
774 weighted mean of 3919±4 Ma (MSWD= 0.45, probability of 0.77).

775 **4.2. U-Pb ages of phosphates**

776 In addition to phosphates from three fragments extracted from the Apollo 14 soil 14161
777 reported in this study, Snape et al (2016a) investigated phosphates in four breccia samples
778 from the same landing site. These four samples gave nearly identical ages (Table 5), with the
779 exception of those obtained for the sample 14321 and four grains (out of 27 analyzed) located
780 in the samples 14305 and 14314. Phosphates from sample 14321 define an age of 3943±5
781 Ma, which appears to be slightly older than the weighted mean of ages 3927±2 Ma defined
782 by other samples. This difference, as well as four older grains found in two other breccias,
783 has been interpreted as a possible mixing of Imbrium ejecta with older material underlying
784 the Fra Mauro formation. Recalculating the original data using the $^{207}Pb/^{206}Pb$ vs. $^{204}Pb/^{206}Pb$
785 intercept, results in a very small (2 to 5 Ma) change in the age estimates, which does not
786 exceed analytical uncertainties (Table 5). Consequently, the small age difference between
787 14321 and all other samples analyzed at Apollo landing sites remains, if an approach using
788 weighted mean calculations, traditionally used in geochronology to determine a combined
789 age derived from several independent age estimates and believed to represent one event, is
790 applied to all available phosphate data.

791 A similarly small age discrepancy was observed in the phosphate data obtained for four
792 samples from the Apollo 17 site (Thiessen et al., 2017). Two poikilitic breccias (76215 and
793 76015) have ages nearly 10 Ma older than aphanitic breccia 72255 and subophitic breccia
794 76065. One of the possible explanations provided by Thiessen et al. (2017) is that the two
795 poikilitic breccias are older and represent an impact event different from that in which the
796 aphanitic and subophitic breccia samples were formed. Very low ^{204}Pb contents in all
797 analyzed samples from the Apollo 17 landing site, reflected in no change of the calculated
798 ages, irrespective of the way the correction for excess Pb is applied (Table 5), suggests that
799 any significant presence of lunar initial Pb in all these grains is unlikely and cannot cause
800 observed difference in ages. However, one of the alternative interpretations discussed by
801 Thiessen et al. (2017) is the possibility of incomplete resetting of the U-Pb system in
802 phosphates from 76215 and 76015, resulting in a small proportion (less than 1% of the total)
803 of Pb accumulated during the pre-impact history of these phosphates remaining inside the
804 grains during the impact, making their ages appear older. Thiessen et al. (2018) also

805 presented U-Pb data for phosphates from an Apollo 12 breccia, which define an age of
806 3925±4 Ma, in the middle of the range given by all analyzed Apollo 14 and 17 samples.

807 Apatite grains from the Apollo 15 samples analyzed in this study, appear to be the youngest
808 in the set of available phosphate ages, at 3915±6 Ma.

809 The combined data from all 12 of samples, where phosphates have been analyzed using U-Pb
810 system, define a weighted mean of 3923±3 Ma, with a relatively high MSWD of 2.5 and low
811 probability of the fit equal to 0.005. These parameters reflect slightly younger Apollo 15
812 phosphates and slightly older phosphates in two Apollo 17 samples, with the total observed
813 range of 15 million years and relatively small errors of a few million years obtained for some
814 samples.

815 **4.3. U-Pb ages of zircon**

816 Two types of zircon grains found in lunar and some terrestrial impactite samples are
817 considered to both represent and date impact events. One is granular-textured zircon
818 composed of a polycrystalline aggregate of zircon crystallites, each a few micrometers across,
819 which are interpreted to reflect the recrystallization of a single zircon grain that existed prior
820 to the impact (e.g., Wittmann et al., 2006; Cavosie et al., 2016; Timms et al., 2017, Erickson
821 et al., 2020). The granular texture commonly preserves the shape of the original zircon grain,
822 and all accumulated radiogenic Pb is expelled from the zircon during impact-related
823 recrystallization, enabling the impact event to be dated directly (e.g., Cavosie et al., 2015;
824 Kenny et al., 2017). Several granular zircon grains have been recognized in lunar samples
825 (e.g. Grange et al., 2013; Crow et al., 2016; Hopkins and Mojzsis, 2015), making possible a
826 direct link between their age and the timing of impacts on the Moon. Of particular interest to
827 the subject of this paper is a granular zircon aggregate surrounding a baddeleyite grain found
828 in a section of Apollo 17 breccia 73217 (Grange et al., 2009). The recalculated age of this
829 aggregate using $^{207}Pb/^{206}Pb$ vs. $^{204}Pb/^{206}Pb$ line-fit approach is estimated as 3922±12 Ma
830 (Table 5). Although within uncertainties, this recalculated age is slightly younger than
831 3929±10 Ma age presented in the original paper by Grange et al. (2009) and closer to the
832 mean age estimates of lithic clasts and phosphates described earlier.

833 The second type of zircon grains interpreted to represent and date impacts directly are
834 crystals growing as an integral part of the mineral assemblage of a crystalline impact-melt
835 matrix (e.g. Gnos et al., 2004; Liu et al., 2012). Examples of such growth, found in some
836 crystalline impact-melt breccia fragments from Apollo 12 samples 12032 and 12033 as well

as in the impact-melt portion of lunar meteorite SaU-169, were analyzed and compared by Liu et al. (2012). Ages of these zircon grains (Table 5) were determined to be 3914±7 (12032 and 12033 high-Th impact melt), and 3920±13 Ma (SaU-169) (Liu et al., 2012). Gnos et al. (2004) reported $^{207}Pb/^{206}Pb$ ages for zircons from the impact-melt phase of SaU-169 that yielded a weighted average age of 3909±13 Ma. In addition, recent study by Zhang et al. (2019) described poikilitic zircon found in the impact melt breccia 73155, which gave an average $^{207}Pb/^{206}Pb$ NanoSIMS age of 3921±14 (Table 5).

Examples of these two types of zircon grains are still relatively rare in lunar samples and some of these grains indicate impacts that predate the 3.9 Ga event. Nonetheless, combining existing sets of zircon analyses that could represent an impact event similar in age to that recorded by the lithic clasts and phosphates results in a weighted mean age of 3917±5 Ma (MSWD=0.59, probability = 0.62).

4.4. Compilation of U-Pb and Pb-Pb data

4.4.1. Homogeneity and median estimate of U-Pb (Pb-Pb) age data set

The presented combined set of U-Pb and Pb-Pb ages near 3.9 Ga, determined with relatively high precision, comprises data for 21 samples of materials that include lithic clasts in three Apollo 14 breccias, one Apollo 16 breccia, phosphates found in eleven breccia samples from four different landing sites, and zircon from two landing sites and a lunar meteorite sample (Table 5). Most of the ages appear to be indistinguishable within analytical uncertainties so that a weighted mean of all data, excluding two Apollo 17 phosphate ages, defines a combined weighted mean age of 3922±2 Ma (95% confidence) with a statistically valid MSWD of 1.6 and probability of 0.06. The two excluded analyses represent two Apollo 17 breccias with the slightly older phosphate ages close to 3.93 Ga. The overall similarity of the ages also implies that the age of phosphates from sample 14305 is indistinguishable from the age of the basaltic clasts in the same breccia. In fact, all ages obtained for Apollo 14 samples (with the exception of 14321) where either phosphates or lithic clasts have been analyzed are indistinguishable within the uncertainties. Similarly, zircon and phosphates from the analyzed Apollo 12 impact-melt breccias give essentially the same results (3914±7 and 3925±4 Ma, respectively).

This overall similarity in ages of clasts, phosphates, and zircon from 21 samples collected at five landing sites (Table 5) suggests that they all could have originated in a single basin-forming event. However, while resulting in a relatively small error, the weighted average

calculation is possibly far from being the best way of estimating the age of this event as it is likely to be biased towards the data with the smaller errors. Therefore, defining a median (rather than a weighted mean), which ignores uncertainties of individual data points, should provide a better estimate of the age based on the combined U-Pb data set. Regardless, the median obtained for 21 analyzed samples is similar to the weighted mean with only a slight change in estimated uncertainties at 3922+3/-2 Ma (95% confidence). This uncertainty of 2-3 million years is clearly much smaller than the variance visible in the data (a range of 21 million years).

Taking into account that the stated aim of this manuscript is to assess the limits for the time interval, which includes ages that cannot be clearly distinguished as representing distinct impact events and also representing the limits at which an age is considered to be an outlier, the more suitable approach would be to calculate interquartile range rather than confidence intervals. This approach, known as Tukey's test, determines the difference between the first and the third quartiles and uses a coefficient of 1.5 to determine the limits for the analyses that can be considered as outliers. For example, taking the interpretation of Apollo 14 samples as representing a single impact event, a median age of 3923 Ma can be determined with the limits at 3914 and 3934 Ma (i.e., the age of this impact can be defined as 3923±11 Ma) from all phosphate data available for this landing site. Adding four dates determined on the basis of Pb-Pb analysis of clasts in three Apollo 14 breccias changes this estimate slightly to 3922±13 Ma (Fig.10). It is clear that sample 14321 is the only potential outlier within the Apollo 14 dataset. It is also clear that all data obtained for zircon and phosphates from all other landing sites fall within these defined age limits and, therefore, can be attributed to the same event (Fig.10). The only possible exception is the age of the breccia 66095, which has a younger but relatively imprecise age of 3909±17 Ma, yet it is still not statistically distinguishable from the impact age established above. Consequently, all 21 age dates could possibly represent a single impact event. Combining all data to calculate the median and the limits results in no change of the best currently possible estimate for this impact, which is determined here as 3922±12 Ma (Fig.11). Considering this estimate, only two ages can be viewed as potential outliers (Fig.11). The first one is the 3943±5 Ma age obtained by Snape et al. (2016a) for phosphates in sample 14321, and supporting their interpretation that this breccia incorporated some of the older material underlying the Fra Mauro formation during the emplacement of Imbrium ejecta at the Apollo 14 landing site. The second, determined by Merle et al. (2014) for the phosphates in sample 14311, is 3938±4 Ma and only just within

902 the uncertainty envelop of 3922±12 Ma (Fig.11). However, distinguishing such small
903 differences can be subjective and dependent on the choice of approach used to define outliers.

904 **4.4.2. Implications of the textural and chemical heterogeneity of the samples**

905 The six different Apollo 14 breccia samples analyzed in this study were collected at opposite
906 sides of the landing area and belong to distinct groups according to different classifications of
907 Apollo 14 breccias. Samples 14303, 14305, 14306, and 14314 were located near the landing
908 module, away from Cone crater and outside of its continuous ejecta, while samples 14321
909 and 14083 were collected on the other side of the landing site near the rim of Cone crater.
910 Consequently, the latter two samples were interpreted as representing pre-Imbrium material
911 mixed with Imbrium ejecta, according to Stöffler et al. (1989), Stöffler (1989), and
912 Stadermann et al. (1991), while the other four could have been formed in the Imbrium impact
913 event. Sample 14321, however, is classified as a fragmental, dark-clast-dominant breccia
914 with coherent to moderately coherent matrix by Wilshire and Jackson (1972), similar to four
915 samples collected near the lunar module (group F-4 of these authors). In contrast, sample
916 14083 appears to belong to the type of breccia with a friable matrix (group F-3 of Wilshire
917 and Jackson, 1972).

918 While lithic clasts investigated in this study clearly predate breccia formation, phosphates can
919 also crystallise from the impact-melt phase. Nevertheless, textural relationships between
920 studied phosphates and the host breccia matrices (i.e., much larger size of phosphate grains as
921 compared to that of the minerals constituting matrix) indicate that the analyzed phosphate
922 grains are xenoclasts that predate breccia formation, similar to lithic clasts. Therefore, the
923 most likely explanation of an overall similarity of ages of different materials across six
924 different samples is resetting of their U-Pb systems. Some of the U-Pb phosphate data
925 obtained for these samples appear to support the suggestion that they represent variable
926 mixing of Imbrium ejecta and older material (e.g. slightly older ages of phosphates from
927 14321). However, the majority of ages determined for both phosphates and lithic clasts
928 indicate that the U-Pb systems in these breccias where profoundly reset as a result of a single
929 thermal pulse, most likely an impact, irrespective of textural variability of the samples or
930 their location. Based on the available data, 3922±12 Ma is interpreted as the best currently
931 available estimate of this impact.

932 Two aphanitic breccia samples collected from the lower slopes of the South Massif at the
933 Apollo 17 landing site (72255 and 73217) provide phosphate and granular zircon ages that

934 are indistinguishable from each other and the Apollo 14 median age of 3922±12 Ma. A
935 similar age is also determined from phosphates in the subophitic breccia 76055, originating at
936 the opposite side of the landing site at the base of North Massif. However, two poikilitic
937 samples (76015 and 76215) give phosphate ages that are approximately ten million years
938 older, if weighted mean ages of the samples are compared. Incomplete resetting of the U-Pb
939 system of these phosphates is more difficult to invoke in the case of these two samples as
940 compared to the Apollo 14 samples, taking into account that the poikilitic breccias represent a
941 hotter melt crystallization environment than the aphanitic samples. Therefore, it is possible
942 that poikilitic breccias from the Apollo 17 site represent an impact that is different from the
943 one that produced the aphanitic breccias and the breccias from the Apollo 14 collection.
944 However, the ages of the two poikilitic breccias are not identified as outliers by Tukey's test
945 made using all Apollo 17 samples or when combined with the Apollo 14 data. Consequently,
946 a clear and unambiguous separation of these ages as representing a separate impact is not
947 supported using currently available data.

948 The two investigated Apollo 15 samples were classified by Ryder and Spudis (1976) as fine
949 grained ophitic/granular melts with some lithic (norite, troctolite) and mineral clasts. They are
950 texturally distinct from all Apollo 14 samples, but have very similar phosphate ages. Textural
951 relationships between phosphates and other constituents of the samples suggest that the
952 analysed phosphates crystallized in plutonic rocks represented by their encapsulating lithic
953 clasts and were reset by the impact that formed the impact melt, and could be the same event
954 that reset phosphates and lithic fragments in Apollo 14 breccias.

955 Breccias 12033 and 66095 from two additional landing sites add further textural and
956 chemical variability to the set of diverse samples that appear to define very similar U-Pb
957 ages. This suggests that the U-Pb system in phosphates, lithic fragments, and rock-forming
958 minerals is relatively easy to reset during impacts. Therefore, it is appropriate to use these
959 phases to date impacts irrespective of the initial composition, origin of the target materials, or
960 thermal history (at least within the temperature range reflected by the different textural types
961 represented by the studied samples from five Apollo landing sites).

962

963 **4.5. Comparison of U-Pb and $^{40}Ar/^{39}Ar$ ages**

964 A total of 49 published original articles containing 259 analyses of impact-related samples
965 acquired using $^{40}Ar/^{39}Ar$ step-heating technique have been examined to enable comparison

966 with U-Pb ages. Detailed description of assessment and recalculation of these data sets is
967 given in Supplementary Materials. Most of the $^{40}Ar/^{39}Ar$ ages were obtained during the 1970s
968 with only a few studies made in the last 20 years. However, 16 out of 29 ages accepted
969 according to the discussed earlier statistical parameters and presented in the final compilation
970 (Table 6) are given in the 3 most recent publications (Dalrymple and Ryder, 1993; 1996;
971 Norman et al., 2006), reflecting the significant improvement of data analysis associated with
972 this analytical technique in the last 20 years. Nevertheless, a significant number of analyses
973 made in earlier research, especially those predating 1976, have been made using monitor
974 samples with the ages that are not updated in the more recent studies. Consequently, while
975 some of these data are of high quality and satisfy statistical parameters proposed here, they
976 are difficult to compare with the more recently obtained ages and, therefore, are excluded
977 from the final compilation. This is particularly related to the Apollo 14 samples, which were
978 not analysed since the early 1970s, with an exception of Stadermann et al. (1991). That paper,
979 however, did not provide information about the standard used to calibrate the irradiation
980 parameters, making it impossible to recalculate these data for the updated monitor ages.
981 Several other papers are missing this information or details related to the degassing steps,
982 preventing statistical assessment of the data. Regardless of these difficulties, a selected set of
983 analyses (Table 6) represents samples with the simplest degassing patterns, which results in
984 the least controversial interpretation of the ages as representing the time of formation of
985 breccia samples during impacts. While all results discussed further have been recalculated
986 using the decay constants from Steiger and Jäger (1977) and Renne et al. (2011), only the
987 latter, which have been calibrated directly against U-Pb ages, is used here for comparison
988 with U-Pb data available for lunar breccia samples.

989 Five poikilitic and subophitic samples from North Massif at Apollo 17 landing site (analysed
990 by Turner and Cadogan, 1975, and Cadogan and Turner, 1976), appear to show similar ages
991 within uncertainties, defining a weighted mean of 3942 ± 36 Ma (MSWD = 0.65, P = 0.62).
992 Seven ages obtained for four aphanitic breccia samples from South Massif are more diverse,
993 most likely reflecting their higher clast content. In particular, two ages of > 4.0 Ga obtained
994 for the fragments from 73215 by Jessberger et al. (1976, 1977) are older than those for other
995 fragments, even one from the same sample. These authors indicated that the age of the oldest
996 fragment is about 100 Ma younger than the assumed age of the source rocks of the clasts and
997 about 100 Ma older than the age likely to represent the formation of the breccia. They
998 therefore proposed that this intermediate age likely represents a mixing between older,

partially degassed clasts and the younger aphanitic matrix. In addition, one of the fragments from 72255 analysed by Dalrymple and Ryder (1996) is slightly older at 3999 ± 40 Ma and can also represent mixing between different components in the sample. Four younger ages define a weighted average of 3923 ± 51 Ma, with MSWD = 1.8 and P = 0.14.

Ten out of twelve accepted ages obtained from Apollo 16 samples were published by Norman et al. (2006). Ten samples can be also put together as a single statistical group, defining a weighted average age of 3913 ± 12 Ma (MSWD = 1.6, P = 0.10). Two samples that appear to be different are both published by Norman et al. (2006). One of these, 61569, is a poikilitic impact melt collected in the eastern part of the landing site (Station 1) and yields a recalculated age of 3846 ± 26 Ma. This sample belongs to the unclassified group of Apollo 16 impact melt breccias according to Korotev (1994). This group consists mainly of a few remaining samples with compositions different from the main groups. Impact melt 61569 is included in this group based on a large compositional scatter observed between three different subsamples. Norman et al. (2006) noted that the younger age of this sample is difficult to reconcile with the ages of other impact melts of their study.

The other sample, 63525-2, is the oldest from the Apollo 16 site (Norman et al., 2006) and is an impact melt from North Ray crater (Station 13). It yields an age of 4239 ± 35 Ma and belongs to group 4 of Korotev (1994), which corresponds to highly aluminous samples with low incompatible element concentrations and is mainly found in the vicinity of North Ray crater, in the northeastern part of the Apollo 16 landing site. Korotev (1994) suggested that the samples from this group "probably represent several small impacts into feldspathic upper crust". Norman et al. (2006) proposed the idea that this age could represent an older event or possibly an incomplete degassing of some clasts, as the North Ray crater samples are also richer in clasts than other Apollo 16 breccias (Ryder and Norman, 1980). This latter explanation would also support the poor reproducibility among the two splits analysed for the sample 63525 (Norman et al., 2006).

The 5 data sets from Apollo 15 landing site presented in the final compilation are from a single publication (Dalrymple and Ryder, 1993) and show similar ages with a weighted mean at 3920 ± 17 Ma (MSWD = 0.1, P = 0.98).

Combining all available $^{40}Ar/^{39}Ar$ data for three landing sites results in twenty-four out of the twenty-nine ages indistinguishable within uncertainty and defining a weighted mean age of 3916 ± 7 Ma (95 % conf., MSWD = 1.1; P =0.13). This estimate is also indistinguishable

1031 from the weighted mean of all U-Pb and Pb-Pb ages of 3922±2 Ma. Applying the median
1032 approach proposed here for the treatment of U-Pb data to all compiled $^{40}Ar/^{39}Ar$ ages also
1033 results in a complete agreement between the two isotope systems, giving median $^{40}Ar/^{39}Ar$
1034 age of 3919 +14/-12 Ma (95% confidence) or 3919±53 Ma, if interquartile range is used to
1035 determine the variance limits for the combined data set. Five $^{40}Ar/^{39}Ar$ ages, mentioned
1036 earlier, are identified as potential outliers.

1037 These results indicate that, irrespective of the approach taken to combine all available
1038 chronological data obtained using U-Pb and $^{40}Ar/^{39}Ar$ systems, 36 out of 41 investigated
1039 breccia samples collected at five different landing sites cannot be distinguished as
1040 representing different impact events within existing analytical uncertainties. Taking into
1041 account wide areal distribution of the samples, this event has to be formation of one of lunar
1042 basins. Linking this age to a specific impact basin, however, is complicated by the multiple
1043 uncertainties associated with the interpretation of the origin of the analyzed samples.

1044

1045 **4.6. Comparing Rb-Sr data with combined U-Pb and $^{40}Ar/^{39}Ar$ data set**

1046 Most of Rb-Sr studies of lunar rocks concentrated on magmatic history of the Moon.
1047 However, several data sets are relevant to the discussion of impact history. Additional details
1048 of reprocessing of these data sets in order to confirm homogenization and update ages using
1049 Rb decay constant of Minster et al. (1982) as well as a short description of the samples is
1050 given in Supplementary Materials. The resulting Rb-Sr isochron ages are shown in Table 7.
1051 The only breccia sample (14321) investigated by several of these studies (e.g. Papanastasiou
1052 and Wasserburg, 1971; Mark et al., 1973) was found to be not completely homogenized with
1053 respect to Rb-Sr system, which is remarkable considering that this is also the only sample at
1054 the Apollo 14 landing site, showing older phosphate U-Pb ages. The rest of the samples from
1055 both Apollo 14 and 16 landing sites investigated using Rb-Sr system are unique and can be
1056 texturally characterised as basalts. However, they have been classified as impact melts based
1057 either on their enrichment in siderophile elements or pieces of breccia attached to the bulk of
1058 the sample. Nevertheless, they do not contain clasts of target rocks and in that respect
1059 probably represent pure impact melt, i.e. very different from the samples analysed using U-Pb
1060 and $^{40}Ar/^{39}Ar$ methods. Three samples presented in Table 7 have ages of 3911 ± 35, 3924 ±
1061 28 and 3993 ± 93 Ma, within the uncertainties of the $^{40}Ar/^{39}Ar$ and U-Pb median ages
1062 described above. The other six samples appear to be about 50 Ma younger, with three of

1063 those from Apollo 16 landing site, where Norman et al. (2006) identified similarly younger
1064 population of different samples using $^{40}Ar/^{39}Ar$ dating, although recalculating their data using
1065 most recent decay constants and monitor ages leaves only one sample (61569) that is clearly
1066 younger than the main group of Apollo 16 samples studied by these authors. Nevertheless,
1067 combined group of these younger samples appear to be very diverse chemically and
1068 texturally, ranging from high-Al to KREEP-rich compositions and poikilitic breccia (sample
1069 investigated by Norman et al., (2006) using $^{40}Ar/^{39}Ar$ dating) to crystallized impact melts
1070 (samples studied using Rb-Sr method). However, their similarity in age may indicate an
1071 impact at about 3850 Ma, different from 3922±12 Ma event.

1072

1073 **4.7. Linking Apollo samples to impact events**

1074 A significant proportion of highland rocks collected by the Apollo missions, including those
1075 evaluated in this study are breccias containing different quantities of rock and mineral
1076 fragments (clasts) welded together by a matrix that represents impact melt recrystallised to
1077 various degrees. Analyses of these samples established that non-mare regions of the Moon
1078 consist of complex, partly shock-melted breccias that have been assembled by impacts.
1079 However, the exact provenance of these breccias remains controversial. Although the general
1080 stratigraphy of the Moon on a large scale appears to be established, origins of samples
1081 collected from each landing site can hypothetically be linked to several impact structures.
1082 Furthermore, each site can potentially also represent material derived from different impacts.
1083 Consequently, while many samples collected by the Apollo missions have been interpreted as
1084 representing the Imbrium impact, this interpretation still relies on a range of assumptions
1085 unique to different samples and landing sites. Arguments for a range of often conflicting
1086 interpretations of different rock formations present on different landing sites as well as origin
1087 of individual samples were made with various success on the basis of remote sensing
1088 observations as well as studies of textural and chemical characteristics of breccias.

1089 Although the Apollo 14 landing site is located 600-800 km from the rim of Imbrium basin,
1090 the Fra Mauro Formation identified at this site has been interpreted as Imbrium ejecta (e.g.,
1091 Swann et al., 1977). This formation appears to be expressed as a series of elongated ridges
1092 that are radial to the Imbrium rim and looks similar to the concentric ridges near the most
1093 prominent ring of the basin. Although the ridges composed by the Fra-Mauro Formation are
1094 covered by, or have surface deposits mixed with, Copernicus ejecta near the Imbrium basin,

1095 interrupting stratigraphic continuity, it is generally accepted that they were formed originally
1096 by material produced by the Imbrium impact (e.g., Wilhelms, 1987).

1097 One of the aims of the Apollo 15 mission was to collect samples from the Montes Apenninus,
1098 which constitute the topographic rim of the Imbrium basin. According to models of crater
1099 development, rim materials should have come from deep parts of the excavation, exposing
1100 pre-Imbrian rocks (including some Serenitatis material) mixed with the Imbrium ejecta.
1101 Nevertheless, although the site is located at the topographic rim of Imbrium basin, it is also
1102 between the rim and intermediate rings of Serenitatis basin. In addition, the set of samples
1103 collected at Apollo 15 landing site has a significant proportion of mare basalts and regolith
1104 breccias that postdate both Imbrium and Serenitatis. Both location of the landing site and
1105 presence of substantial volcanic component complicate the interpretation of the several
1106 impact melt breccias that have been identified among the samples (e.g., Ryder and Spudis,
1107 1987).

1108 The variability of Apollo 16 samples and the significant distance of the landing site from the
1109 major basins, compared to some other landing sites, makes these samples the most difficult to
1110 link to particular impact structures. The two units sampled during the Apollo 16 mission are
1111 the Cayley formation and Descartes formation. Wilhelms et al. (1987) argued that the Cayley
1112 formation was emplaced during the Imbrian period, but could consist of reworked material
1113 from the Nectaris impact. The Descartes formation was interpreted as originating (at least
1114 partly) from the Nectaris basin (Head, 1972; Wilhelms, 1972), although contribution from
1115 Imbrium could not be completely excluded (Wilhelms et al., 1987).

1116 The Apollo 17 site was selected to sample materials from the Serenitatis basin (Wilhelms et
1117 al., 1987), as the proximity of the site to the basin and geologic interpretations before the
1118 mission supported a view that the sampled materials should originate from this impact.
1119 Nevertheless, as a consequence of complexities in the melt breccia samples, including the
1120 presence of at least two major textural types of breccia matrices, and new interpretations of
1121 basin stratigraphy and the origin of deposits in the Apollo 17 region (Spudis et al., 2011), the
1122 basin of origin of the Apollo 17 samples is less clear.

1123 The Apollo 12 landing was in southeastern Oceanus Procellarum on a mare basaltic surface,
1124 but along a ray associated with Copernicus crater (Spudis and Pieters, 1991; Wilhelms,
1125 1987). Samples collected by the mission are dominated by mare basalts, although some are
1126 regolith breccias and at least one (12013) is a complex polymict impact breccia that appears

to be a mixture of granitic rock and more mafic and KREEP-rich impact melts. Nevertheless, clear stratigraphic control and knowledge of provenance are absent for the non-Mare components of Apollo 12 samples, which probably were delivered to the Apollo 12 site by one or more additional impacts following their origin in a basin-forming event.

Initial examination of returned Apollo 14 samples indicated that most of the 124 specimens larger than one gram are fragmental rocks consisting of variety of mineral and lithic clasts, ranging from plutonic and basaltic rocks to older generations of breccia, with matrices characterised by different textures (e.g. Wilshire and Jackson, 1972). Four groups were distinguished among the samples in early descriptions. Breccias bearing regolith components were interpreted as representing post Imbrium modification of locally derived material (F1-type breccias, e.g. Wilshire and Jackson, 1972, Chao et al., 1972; Lindsay, 1975). Other three groups (F2-type, moderately coherent and dominated by the light-colored clasts; F3-type, friable – dominated by dark clasts; and F4-type, moderately coherent and dominated by dark clasts) are abundant in the collection from the Apollo 14 site. The F3- and F4-types are also abundant near Cone crater, which excavated the Fra Mauro formation to a depth of approximately 75 m. Therefore, F3- and F4-types are interpreted to represent deeper stratigraphic layers within the sequence underlying the Apollo 14 site; however, Wilshire and Jackson (1972) argued that because the major ridge structure of Fra Mauro formation was not disturbed significantly by the later impacts, these breccias still represent Fra Mauro deposits. Variable degrees of re-equilibration displayed by the Apollo 14 breccia matrices were then interpreted to reflect a relatively slow differential cooling in a single impact ejecta blanket (Warner, 1972; Williams, 1972). Temperature estimates based on this model suggested heating of most equilibrated breccias to about 1100-1300 $^{\circ}$C (e.g. Williams, 1972; Lindsay, 1975)

This interpretation of Apollo 14 breccias implies that the F2, F3, and F4 types of breccias identified by Wilshire and Jackson (1972) represent the Fra Mauro Formation and provided that this formation represents the Imbrium ejecta blanket, their ages can be used to determine the age of the Imbrium impact. However, in a series of papers, Stöffler et al. (1989), Stöffler (1989), Stadermann et al. (1991) introduced a different interpretation of both textural features observed in the Apollo 14 breccias and distribution of different breccia types relative to the Cone crater. They argued that a group of breccia samples collected near the crater represents a stratigraphic unit that predates the Imbrium impact, and that only those samples collected further from the crater, which contain a significant proportion of clasts of impact melt

lithologies and originating from a sub-regolith layer, are representative of the Imbrium impact event.

Despite the existing controversy, there is a general agreement that the sampled material represents, at least in part, Imbrium ejecta, which was significantly mixed with local older material during deposition. Providing that mixing during ballistic sedimentation was accompanied by a significant increase in temperature, which is indicated by re-equilibration reaction textures visible in most of the samples, partial or complete resetting of different isotopic system should have been associated with this event. The set of ages presented here appears to confirm this view, with the majority of samples showing similar ages within the ±12 Ma limits, irrespective of the observed textural differences and location. This similarity can indicate that all investigated samples were formed or profoundly modified by a single impact. Alternatively, if they originated in different impacts, these impacts should all have been confined to a narrow time window of ±12 Ma.

Interpretation of the origin of Apollo 17 breccias is equally controversial, which is underlined by the presence of two textural groups of samples, one with matrices ranging from ophitic and sub-ophitic to poikilitic and indicating crystallisation from hot melts, and the other, with aphanitic matrices, suggesting rapid cooling. Differences between two textural types are further supported by existing differences in clast contents and distinct areal distributions at the landing site, with poikilitic samples found near the North Massif and aphanitic breccias found near the slopes of the South Massif. All these differences have been used as an argument for the formation of Apollo 17 breccias in multiple impacts (Ryder et al., 1975; Spudis and Ryder, 1981). Spudis and Ryder (1981) also suggested that the poikilitic impact melt breccias from the Apollo 17 landing site represent ejecta from the Serenitatis impact, but in general the site has recorded a complex multi-impact history, even if it is dominated by Serenitatis impact ejecta. An alternative interpretation appeals to compositional similarity of the matrices of the samples to low-K KREEP (e.g., Ryder and Wood, 1977; Winzer et al., 1977). This general compositional uniformity of the samples was taken as evidence of emplacement as a result of a single impact (e.g., Wilhelms, 1987). The apparent absence of age difference between the aphanitic and poikilitic breccia groups has also been used to support this interpretation. This absence of an age difference is further reinforced by compilation of the most recent chronological data, which indicate that while poikilitic samples can be slightly (~10 Ma) older than aphanitic breccias, but these textural types cannot be confidently separated into two distinct groups on the basis of their ages.

1193 Consequently, they could have formed in a single impact. Similar to Apollo 14 samples, if
1194 poikilitic and aphanitic breccias originated in two separate impacts, the timing of these
1195 impacts must be confined within the ±12 Ma limits.

1196 Korotev (1994) separated the impact-melt breccias of Apollo 16 into four different groups
1197 based on major and trace element analyses of approximately 110 samples and following the
1198 scheme adopted by McKinley et al. (1984). The groups correlate with increasing Al content
1199 so that more mafic and KREEP-rich samples that coincide with the Cayley formation
1200 correspond to groups 1M and 1F, whereas the more feldspathic, KREEP-poor samples
1201 originating within the Descartes formation are included in groups 2DB and 2NR. Lithophile
1202 elements in all groups display trends that can be explained by a variable mixing with
1203 anorthosite. In addition, some differences in incompatible elements observed within the
1204 groups allowed Korotev (1994) to subdivide group 1 and some group 2 samples into more
1205 mafic and more feldspathic melt rocks. The remaining group 2 samples were also split into
1206 two subgroups that appear to show a specific spatial distribution, with one type associated
1207 with North Ray crater while the other was probably excavated by South Ray crater. Finally,
1208 there is a visible difference between groups 1 and 2 (western trend) and groups 3 and 4
1209 (eastern trend) on a plot of Sm vs. Sc (Korotev, 1994) that distinguish these groups. There is
1210 some degree of correlation between chemical groups and textures of impact melts: group 1
1211 melts having poikilitic textures; group 2, poikilitic to ophitic and interstitial textures; group 3,
1212 ophitic to interstitial textures; and group 4, microporphyritic to microgranular textures. The
1213 transition may be linked to the overall increase in feldspar content of the melts.

1214 Norman et al. (2006) investigated 25 samples of Apollo 16 impact-melt breccias dividing
1215 them into four textural groups and arguing for an origin in different impacts ranging in age
1216 between 3.75 and 3.96 Ga, based on $^{40}Ar/^{39}Ar$ dating. However, filtering of $^{40}Ar/^{39}Ar$ data,
1217 presented here, identifies that only ten of these ages qualify as true plateau or mini-plateau
1218 ages with 8 of those defining a single age population of 3912 ± 13 Ma (P=0.16). This
1219 population includes samples representing several distinct types of impact melts identified by
1220 Korotev (1994). Consequently, there is no simple relationships between textures, chemistry,
1221 and ages of Apollo 16 impact melt breccias, which makes finding a unique interpretation of
1222 the samples difficult. It is even more difficult to link all or some Apollo 16 samples to a
1223 specific impact basin (or basins), such as Imbrium or Nectaris, given the ambiguities arising
1224 from the absence of clear stratigraphic control on the origin of the Descartes and Cayley
1225 formations. Korotev (1994) did not provide a unique explanation for the observed variation in

1226 the compositions of mafic impact melts at the Apollo 16 landing site. Instead, he compared
1227 four different scenarios, including (i) two or more basin-scale impacts, (ii) a single basin-
1228 scale impact, (iii) a single local impact, and (iv) multiple local impacts. He highlighted
1229 specific problems with all of these interpretations, concluding that none of the scenarios can
1230 explain all variations in chemical compositions without invoking some improbable
1231 assumptions about the impactors, impact events, or composition of possible components
1232 likely to be mixed to produce specific impact melts. There is a possibility indicated by the
1233 ages provided by Norman et al. (2006) that at least some of the more feldspathic impact melts
1234 present in the collection reflect local impacts, whereas the mafic melts are linked to the basins
1235 or a basin, as indicated by the general age similarity of the majority of analysed samples.

1236 The majority of Apollo 15 impact melts have the composition of low-K Fra Mauro basalt,
1237 contain a relatively low proportion of clasts, and exhibit textures varying from aphanitic to
1238 fine-grained ophitic and micro-poikilitic. Ryder and Spudis (1987) analyzed the major and
1239 trace element concentrations of 14 impact melt samples from Apollo 15 and classified them
1240 into 5 groups (A-E) according to chemistry. All investigated samples, with the exception of
1241 one are KREEP-rich, but show significant concentration variations of some trace elements
1242 such as Ti, Sm, and Sc, which led Ryder and Spudis (1987) to conclude that they represent at
1243 least four separate impact events. However, Korotev (1998) argued that the major- and trace-
1244 element geochemistry of all low-K and medium-K Fra Mauro basalts (melt rocks) and very-
1245 high-Al (VHA) basalts (melt rocks) from the Apollo 16 can be explained as a mixture of
1246 Apollo 15 KREEP basalt, highly magnesian olivine, and feldspathic upper crust. This
1247 explanation supports the possibility that some of the compositionally variable impact melt
1248 samples can have been formed by a single impact event.

1249 It is becoming increasingly clear that in spite of existing preferred interpretation for each
1250 Apollo landing site in relation to the formation of several major impact basins, the
1251 stratigraphic relationships remain ambiguous with regard to linking specific samples to their
1252 basin of origin.

1253 Using compositional and textural variations observed in the melt breccias to link particular
1254 samples to specific impact events relies on the assumption that the similarity of chemical
1255 composition (and texture) of different samples of impact melt means formation in a single
1256 impact event, while differences are interpreted as evidence of multiple impacts. The pitfalls
1257 of this assumption were discussed previously (e.g. Haskin et al., 1998; Korotev, 1994). The
1258 assumption of homogenization of melt in an impact event comes from the early studies of

terrestrial impact melts; however, Dressler and Reimold (2001) reviewed impact melt rocks and glasses from a variety of terrestrial impact craters and suggested that variability in melt rock bulk composition within single impact structures is quite common. In addition, Haskin et al. (1998) argued that melt sheets produced by the significantly larger basin-forming events on the Moon may not be as homogenous as those studied on the Earth. Many of the impact-melt breccia matrices from Apollo 12, 14, 15, 16, and 17 are KREEP-bearing or KREEP-rich. That led Haskin et al. (1998) to conclude that all Apollo landing sites may be dominated by the ejecta of a single impact (most likely Imbrium) irrespective of some second order variations in chemical composition and texture of the collected impact-melt samples. However, this interpretation is also not free of ambiguity, as the general similarity of compositions may simply reflect the abundance of KREEP materials in the Procellarum KREEP terrane so that any basin-forming event in this region could potentially penetrate the crust and remelt KREEP-rich rocks. In that case, the significant compositional differences of the Apollo 16 samples could be taken as support for an origin of the more feldspathic impact-melt groups outside of the Procellarum KREEP terrane.

Similar opposing arguments can be made with respect to applicability of textural homogeneity or heterogeneity to the purpose of identifying cogenetic samples formed by a single impact. Generally, different textures reflect differences in the initial temperature and cooling history of impact melts, and these thermal effects are linked to the initial proportion and composition of clasts and impact melt as well as the initial position of the samples within the impact ejecta deposits. A difference in the textures therefore cannot be interpreted unambiguously in support of different impacts. Likewise, similarity of texture cannot be taken as evidence of formation in the ejecta deposits of a single impact event. The ambiguity is especially exaggerated by the fact that none of the Apollo samples were collected from an outcrop and their original location relative to other samples is unknown.

4.8. The age of the Imbrium impact

While there are still various degrees of ambiguity in linking Apollo impact-melt samples to the specific impacts on the basis of remote sensing observations and studies of chemical and textural variability of the samples, significant volume of chronological data obtained using different isotope systems and applied to different constituents (minerals, matrixes and rock fragments) of the breccias collected from five Apollo landing sites indicates a narrow age

range for the formation interval of these samples. While similarity of the samples within this range is evident irrespective of the statistical approach taken to combine individual ages, 3922±12 Ma median with the limits determined from the combined U-Pb data set using interquartile method is advocated here as the best way to identify outliers (i.e. samples that clearly fall out of the group of samples that can be interpreted as representing single impact event). Importantly, consistent similarity of U-Pb and $^{40}Ar/^{39}Ar$ ages in multiple samples from different landing sites covering a substantial area on the near side of the Moon suggests that these samples originated in a single event that was large enough to have formed one of the lunar impact basins. Any alternative, explanation would either require multiple basin forming events taking place within the narrow limits of ±12 Ma or a barrage of a smaller impacts at each landing site within this time interval. Both interpretations would imply a very short spike in the flux of impactors, supporting an extreme "Terminal Lunar Cataclysm" version of impact flux models, however, both are also difficult to reconcile with the modern interpretation of lunar stratigraphy. Consequently, our preferred interpretation is that 3922±12 Ma defines the best confidence interval for the age of a single impact basin on the Moon. As discussed above, difficulties with linking individual samples to the rock formations identified at different landing sites, as well as linking these formations to the specific impact basins prevents a completely unambiguous identification of this 3922±12 Ma basin. Nevertheless, many arguments based on textural and chemical evidence as well as remote observations indicate that this basin is most likely to be Imbrium. In particular, it is generally agreed that Apollo 14 landing site samples represent part of Imbrium ejecta blanket that possibly reworked older material. The latter is supported by the similarity of ages of different breccia samples from this site. If the interpretation of 3922±12 Ma age as time of Imbrium formation is correct, then a total of 38 samples from five landing sites analyzed using U-Pb, $^{40}Ar/^{39}Ar$ and Rb/Sr systems can be viewed as formed by this impact.

5. Conclusions

U-Pb ages of impact-melt breccias, phosphates, and zircon grains from more than 20 different samples from five Apollo landing sites and one meteorite sample appear to support a profound resetting of the U-Pb system during a single impact event. The timing of this event is constrained as a median of individual ages obtained for these samples and is equal to 3922±12 Ma. The ±12 Ma uncertainty was determined using Tukey's test for possible outliers. This approach is taken to offer a more robust estimate of the age as it provides a

1324 better reflection of scatter observed in the group of investigated samples and is not as biased
1325 towards the individual ages with smaller uncertainties, as compared to the commonly used
1326 weighted mean calculations. Applying the latter to the same set of data produces a similar
1327 age, but much smaller uncertainty of ±2 Ma. This weighted mean approach appears to be less
1328 reliable, taking into account that one of the main aims of this study is to establish limits
1329 beyond which an age of a sample can be considered to be different from that of the main
1330 identified group.

1331 Filtering and updating the existing set of $^{40}Ar/^{39}Ar$ data confirms a general similarity of
1332 $^{40}Ar/^{39}Ar$ and U-Pb ages. Twenty-four additional samples from Apollo 15, 16, and 17 landing
1333 sites with the $^{40}Ar/^{39}Ar$ ages define a weighted mean age of 3916 ± 7 Ma (95 % conf.,
1334 MSWD = 1.1; P =0.13) and a median age of 3919 +14/-12 Ma, both in close agreement with
1335 the confidence interval obtained using the U-Pb system and suggesting that the two
1336 techniques have dated the same event. Three additional Rb/Sr ages also overlap within error
1337 with the U-Pb and $^{40}Ar/^{39}Ar$ confidence intervals. $^{40}Ar/^{39}Ar$ data also confirm the previous
1338 observation that some aluminous Apollo 16 breccias may represent a younger (by ~50 Ma)
1339 impact and an older age of sample 63525 (Norman et al., 2006). In addition, Rb-Sr ages of
1340 several samples from Apollo 14 and 16 landing sites, interpreted as representing impact melt,
1341 show a similar younger age, identifying a combined population of seven samples that fall
1342 outside of the 3922±12 Ma limits.

1343 It is important to stress that the chronological data indicate that the majority of the
1344 investigated samples formed in a single impact at 3922±12 Ma or a series of impacts
1345 confined within a narrow (24 Ma) time interval. It is not possible to choose between these
1346 two possibilities; however, the obtained age and the limits provide a means to distinguish
1347 samples that fall outside this narrow interval.

1348 While this interpretation of ages of breccia samples appears to be robust, aligning these ages
1349 to a specific impact or impacts is less definitive and relies on the available interpretation of
1350 lunar stratigraphy and establishing links between the samples and rock formations identified
1351 on the Apollo landing sites as well as their relation to specific impact events. This
1352 interpretation is gradually changing based on the newly available remote sensing data.
1353 However, there is no complete overhaul of the ideas developed during earlier stages of lunar
1354 exploration and the earlier interpretations remain largely unchallenged. Based on these
1355 interpretations we tentatively assign 3922±12 Ma to Imbrium impact. This assignment
1356 follows many arguments that support a link between multiple breccias from different Apollo

landing sites and this impact event. The proposed age range of 3922±12 Ma suggests that the currently analyzed samples could all have been formed as part of Imbrium ejecta, with the possible exception of phosphates from samples 14321 and 14311. Even if a group of breccia samples identified here was formed by a series of closely timed impacts, it is likely that Imbrium also formed within the limits defined above.

Given that the majority of the samples collected from five different landing sites can plausibly have been formed by the Imbrium impact, it is also appears to be highly likely that the KREEP-rich material present at the surface on the near side of the Moon, and referred to as the Procellarum KREEP terrane, is a product of the Imbrium basin forming impact. This likelihood also supports the suggestion (e.g., Haskin et al., 1998) that a significant proportion of the Apollo breccia collection is biased towards Imbrium ejecta. In addition, several persisting issues related to the interpretation of samples from different landing sites can be re-evaluated in light of the relatively narrow range of ages obtained for different samples (±12 Ma). For example, poikilitic and aphanitic breccias from the Apollo 17 landing site cannot be regarded as formed in separate impact events based solely on their chronology. If they did form as a result of different impacts, these impacts must have been timed closely within this range. The presence of outliers in a small group of samples from the Apollo 14 landing site supports the suggestion that the Fra Mauro formation may represent a mixture of Imbrium ejecta and older underlying material. The minimum age of this material is only 10 to 15 Ma older than the ejecta.

In the future it is probably worth focusing some attention on the samples that are different from the main group to verify and better constrain their ages. The added age data for these samples would likely yield additional information relevant to a fuller understanding of the impact history of the Moon.

Acknowledgements

We would like to thank Barbara Cohen and anonymous reviewer for thoughtful comments that helped to improve the manuscript. AAN, TL, DL and YW acknowledge support for the pre-research Project on Civil Aerospace Technologies No. D020205 funded by CNSA. DL and TL acknowledge funding by grants from the National Natural Science Foundation of China (41842045, 41603056). MJW and AAN acknowledge funding by grants from the Knut and Alice Wallenberg Foundation (2012.0097) and the Swedish Research Council (VR 621-2012-4370). BLJ acknowledges support from the McDonnell Center for the Space Sciences, Washington University; and NASA grant NNX07AI44G (R. L. Korotev) for the initial mineral and geochemical characterization of samples from 12032, 12033, 14161, and SaU-169 at Washington University. We also acknowledge ARC funding for the Tescan Mira3 FE-SEM (ARC LE130100053) at the John de Laeter Centre, Curtin University.

References

Baksi A.K., 2007. A quantitative tool for evaluating alteration in undisturbed rocks and minerals – I: water, chemical weathering and atmospheric argon. In The origin of melting anomalies, plates, plumes and planetary processes (eds G.R. Foulger and D.M. Jurdy) Geol. Soc. Amer. Spec. Pap. 430, pp 285–304.

Baldwin, R.B., 2006. Was there ever a Terminal Lunar Cataclysm?. With lunar viscosity arguments. Icarus 184, 308–318.

Bottke, W.F., Norman, M.D., 2017. The Late Heavy Bombardment. Annu. Rev. Earth Planet. Sci. 45, 619–647.

Cadogan P.H. and Turner G., 1976. The chronology of the Apollo 17 Station 6 boulder. Proc. Lunar Planet. Sci. Conf. 7th, 2267–2285.

Cavosie AJ, Erickson TM, Timms NE, Reddy SM, Talavera C, Montalvo SD, Pincus MR, Gibbon RJ, Moser D., 2015. A terrestrial perspective on using ex situ shocked zircons to date lunar impacts. Geology 43(11):999-1002

Cavosie AJ, Timms NE, Erickson TM, Hagerty JJ, Hörz F. 2016. Transformations to granular zircon revealed: Twinning, reidite, and ZrO_2 in shocked zircon from Meteor Crater. Geology 44(9), 703-706.

1413 Chao E.C.T., Minkin J.A. and Best J.B., 1972a. Apollo 14 breccias: General characteristics
1414 and classification. Proc. 3rd Lunar Sci. Conf. 645-659.

1415 Cherniak D. J., Lanford W. A. and Ryerson F. J., 1991. Lead diffusion in apatite and zircon
1416 using ion implantation and Rutherford backscattering techniques. Geochim. Cosmochim.
1417 Acta 55, 1663-1673.

1418 Crow C. A., McKeegan K. D. and Moser D. E., 2017. Coordinated U-Pb geochronology,
1419 trace element, Ti-in-zircon thermometry and microstructural analysis of Apollo zircons.
1420 Geochim. Cosmochim. Acta 202, 264-284.

1421 Dalrymple G.B. and Ryder G., 1993. ^{40}Ar-^{39}Ar age spectra of Apollo 15 impact melt rocks by
1422 laser step-heating and their bearing on the history of the lunar basin formation. J.
1423 Geophys. Res. 98, 13085–13095.

1424 Dalrymple G.B. and Ryder G., 1996. Argon-40/argon-39 age spectra of Apollo 17 highlands
1425 breccia samples by laser step heating and the age of the Serenitatis basin. J. Geophys.
1426 Res. 101, 26069–26084.

1427 Deutsch A. and Stöffler D., 1987. Rb-Sr analyses of Apollo 16 melt rocks and a new age
1428 estimate for the Imbrium basin: Lunar basin chronology and the early heavy
1429 bombardment of the Moon. Geochim. Cosmochim. Acta 51, 1951–1964.

1430 Devine J.M., McKay D.S. and Papike J.J., 1982. Lunar regolith: Petrology of the <10 micron
1431 fraction. Proc. 13th Lunar Planet. Sci. Conf. in J. Geophys. Res. 87, A260-A268.

1432 Dressler B. O. and Reimold W. U. 2001. Terrestrial impact melt rocks and glasses. Earth-
1433 Science Reviews 56:205–284.

1434 Erickson T.M., Kirkland C.L., Timms N.E., Cavosie A.J. and Davison T.M. 2020. Precise
1435 radiometric age establishes Yarrabubba, Western Australia, as Earth's oldest recognised
1436 impact structure. Nature Comms. 11, 300

1437 Finkelman R.B., 1973. Analysis of the ultrafine fraction of the Apollo 14 regolith. Proc. 4th
1438 Lunar Sci. Conf. 179-189.

1439 Gnos E., Hofmann B. A., Al-Kathiri A., Lorenzetti S., Eugster O., Whitehouse M. J., Villa I.
1440 M., Jull A. J. T., Eikenberg J., Spettel B., Krähenbühl U., Franchi I. A. and Greenwood
1441 R.C., 2004. Pinpointing the source of a lunar meteorite: implications for the evolution of
1442 the Moon. Science 305, 657-659.

1443 Grange, M.L., Nemchin, A.A., and Pigeon, R.T., 2013, The effect of 1.9 and 1.4 Ga impact
1444 events on 4.3 Ga zircon and phosphate from an Apollo 15 melt breccia. Journal of
1445 Geophysical Research: Planets, 118 (10), 2180-2197.

1446 Grange, M.L., Nemchin, A.A., Pidgeon, R.T., Timms, N., Muhling, J.R., and Kennedy, A.K.,
1447 2009, Thermal history recorded by the Apollo 17 impact melt breccia 73217.
1448 Geochimica Et Cosmochimica Acta, 73 (10), 3093-3107.

1449 Haskin L.A., Korotev R.L., Rockow K.M. and Jolliff B.L., 1998. The case for an Imbrium
1450 origin of the Apollo thorium-rich impact-melt breccias. Meteor. & Planet. Sci. 33, 959-
1451 975.

1452 Haskin, L. A., B. E. Moss, W. B. McKinnon, 2003. On estimating contributions of basin
1453 ejecta to regolith deposits at lunar sites. Meteorit. Planet. Sci. 38, 13-33.

1454 Head J.W., 1972. Small-scale analogs of the Cayley Formation and Descartes Mountains in
1455 impact-associated deposits. Apollo 16 preliminary science report: NASA Report SP-315,
1456 chap. 29, part C, 29-16–29-20

1457 Head, J.W., 1974. Stratigraphy of the Descartes region /Apollo 16/ - Implications for the
1458 origin of samples. Moon 11, 77–99.

1459 Hertogen, J., Janssens, M.J., Takahashi, H., Palme, H. and Anders, E., 1977. Lunar basins
1460 and craters - Evidence for systematic compositional changes of bombarding population,
1461 Lunar & Planetary Science Conference. Proc. 8th Lunar Sci. Conf. 17-45.

1462 Hopkins M. D. and Mojzsis S. J., 2015. A protracted timeline for lunar bombardment from
1463 mineral chemistry, Ti thermometry and U–Pb geochronology of Apollo 14 melt breccia
1464 zircons. Cont. Mineral. Petrol. 169(3), 1-18.

1465 Jessberger E.K., Horn P. and Kirsten T., 1975. 39Ar-40Ar dating of lunar rocks: A
1466 methodical investigation of mare basalt 75075 (abs). Lunar Sci. VI, 441-443. Lunar
1467 Planetary Institute, Houston.

1468 Jessberger E.K., Kirsten T. and Staudacher Th, 1977. One rock and many ages – Further K-
1469 Ar data on consortium breccia 73215. Proc. Lunar Planet. Sci. Conf. 8th, 2567–2580.

1470 Jessberger E.K., Kirsten T. and Staudacher Th., 1976. Argon-argon ages of consortium
1471 breccia 73215. Proc. Lunar Planet. Sci. Conf. 7th, 2201–2215.

1472 Jessberger E.K., Staudacher Th., Dominik B. and Kirsten T., 1978. Argon-argon ages of
1473 aphanite samples from consortium breccia 73255. Proc. Lunar Planet. Sci. Conf. 9th,
1474 841–854.

1475 Jolliff, B. L., 1998. Large-scale separation of K-frac and REEP-frac in the source regions of
1476 Apollo impact-melt breccias, and a revised estimate of the KREEP composition.
1477 International Geology Review 40, 916-935.

1478 Jolliff, B. L., R. L. Korotev, L. A. Haskin, 1991. Geochemistry of 2-4 mm particles from
1479 Apollo 14 soil (14161) and implications regarding igneous components and soil-forming
1480 processes. Proceedings of the Lunar and Planetary Science Conference 21, 193-219.

1481 Jourdan F., Renne P.R., Reimold W.U., 2009. An appraisal of the ages of terrestrial impact
1482 structures. Earth Planet. Sci. Lett. 286, 1–13.

1483 Jourdan F., Verati C. and Féraud G., 2006. Intercalibration of the Hb3gr $^{40}Ar/^{39}Ar$ dating
1484 standard. Chem. Geol. 231, 177–189.

1485 Joy, K.H., Kring, D.A., Bogard, D.D., McKay, D.S., Zolensky, M.E., 2011. Re-examination
1486 of the formation ages of the Apollo 16 regolith breccias. Geochim. Cosmochim. Acta 75,
1487 7208–7225.

1488 Kaiyun, C., Honglin, Y., Zhian, B., Chunlei, Z. and Mengning, D., 2014. Precise and
1489 Accurate In Situ Determination of Lead Isotope Ratios in NIST, USGS, MPI-DING and
1490 CGSG Glass Reference Materials using Femtosecond Laser Ablation MC-ICP-MS.
1491 Geostandards and Geoanalytical Research 38, 5-21.

1492 Kenny, G., Morales, L. F., Whitehouse, M. J., Petrus, J. A., Kamber, B. S., 2017, The
1493 formation of large neoblasts in shocked zircon and their utility in dating impacts.
1494 Geology, 45 (11), 1003-1006.

1495 Kenny,G.G.,Schmieder,M.,Whitehouse,M.J.,Nemchin,A.A.,Morales,L.F.,Buchner,E.,
1496 Bellucci,J.J.,Snape,J.F.,2019.AnewU–Pbageforshock-recrystallisedzirconfrom
1497 theLappajärviimpactcrater,Finland,andimplicationsfortheaccuratedatingof
1498 impactevents.Geochim.Cosmochim.Acta245,479–494

1499 Koppers A.P., 2002. ArArCALC—software for $^{40}Ar/^{39}Ar$ age calculations. Computers &
1500 Geosciences 28, 605–619.

1501 Korotev R.L., 1998. Concentrations of radioactive elements in lunar materials. J. Geophys.
1502 Res. 103, 1691-1701.

1503 Korotev, R. L., 1994. Compositional variation in Apollo 16 impact-melt breccias and
1504 inferences for the geology and bombardment history of the Central Highlands of the
1505 Moon. Geochimica et Cosmochimica Acta 50, 3931-3969.

1506 Li, Q.-L., Li, X.-H., Wu, F.-Y., Yin, Q.-Z., Ye, H.-M., Liu, Y., Tang, G.-Q., Zhang, C.-L.,
1507 2012. In-situ SIMS U–Pb dating of phanerozoic apatite with low U and high common
1508 Pb. Gondwana Res., Advances in High-Resolution Ion-Microprobe Geochronology 21,
1509 745–756.

1510 Lindsay, J.F., 1976, Lunar Stratigraphy and Sedimentology. Elsevier, Amsterdam, 302 p.

1511 Liu D., Jolliff B. L., Zeigler R. A., Korotev R. L., Wan Y., Xie H., Zhang Y., Dong Y. and
1512 Wang W., 2012. Comparative zircon U-Pb geochronology of impact melt breccias from
1513 Apollo 12 and lunar meteorite SaU 169, and implications for the age of the Imbrium
1514 impact. Earth Planet. Sci. Lett. 319, 277-286.

1515 Ludwig K. R., 2008. User's Manual for Isoplot 3.60, A geochronological toolkit for
1516 Microsoft Excel. Berkeley Geochronological Center Special Publication 4, Berkeley,
1517 California: Berkeley Geochronological Center.

1518 Ludwig K.R., 2003. User's manual for Isoplot 3.00. Berkeley Geochronological Center
1519 Special Publication, p. 74.

1520 Mahon K.I., 1996. The new York regression: application of an improved statistical method to
1521 geochemistry. Int. Geol. Rev. 38, 293–303.

1522 Mark R.K., Cliff R.A., Lee-Hu C.-N. and Wetherill G.W., 1973. Rb-Sr studies of lunar
1523 breccias and soils. Proc. Lunar Planet. Sci. Conf. 4th, Geochim. Cosmochim. Acta Suppl.
1524 4, 1785–1795.

1525 Mark R.K., Lee-Hu C.-N. and Wetherill G.W., 1974. Rb-Sr age of lunar igneous rocks 62295
1526 and 14310. Geochim. Cosmochim. Acta 38, 1643–1648.

1527 Marvin U.B., Lindstrom M.M., Bernatowicz T.J., Podosek F.A. and Sugiura N., 1987. The
1528 composition and history of breccia 67015 from North Ray Crater. Proc. 17th Lunar
1529 Planet. Sci. Conf., J. Geophys. Res., 92, B4, E471–E490.

1530 McDougall I. and Harrison T.M., 1999. Geochronology and thermochronology by the
1531 $^{40}Ar/^{39}Ar$ method. Oxford Univ. press, Oxford, p. 269.

1532 Mcgee, P.E., Simonds, C.H., Warner, J.L. and Phinney, W.C., 1979. Introduction to the
1533 Apollo collections: Part 2: Lunar breccias. Nasa Sti/recon Technical Report N 80.

1534 McKay G.A., Wiesmann H., Nyquist L.E., Wooden J.L. and Bansal B.M., 1978. Petrology,
1535 chemistry, and chronology of 14078: Chemical constraints on the origin of KREEP.
1536 Proc. Lunar Planet. Sci. Conf. 9th, 661–687.

1537 McKinley J.P., Taylor G.J., Keil K., Ma M.-S. and Schmitt R.A., 1984. Apollo 16: Impact
1538 sheets, contrasting nature of the Cayley Plains and Descartes Mountains, and geologic
1539 history. Proc. 14th Lunar Planet. Sci. Conf. in J. Geophys. Res. 89, B513-B524.

1540 Mercer, C. M., K. V. Hodges, B. L. Jolliff, M. C. van Soest, J.-A. Wartho, J. R. Weirich,
1541 2019. Exploring the variability of argon loss in Apollo 17 impact melt rock 77135 using
1542 high spatial resolution 40Ar/39Ar geochronology. Meteorit. Planet. Sci. 54, 1-19.

1543 Merle, R.E., Nemchin, A.A., Grange, M.L., Whitehouse, M.J. and Pidgeon, R.T., 2014. High
1544 resolution U-Pb ages of Ca-phosphates in Apollo 14 breccias: Implications for the age of
1545 the Imbrium impact. Meteoritics & Planetary Science 49, 2241-2251.

1546 Minster J.-F, Birck J.-L., Allegre, C. J., 1982. Absolute age of formation of chondrites
1547 studied by the 87Rb-87Sr method. Nature 300, 414–419.

1548 Muehlberger W.R., Horz F., Seiver J.R. and Ulrich G.E., 1980. Mission objectives for
1549 geological exploration of the Apollo 16 landing site. In Proc. Conf. on Lunar Highlands
1550 Crust, 1-49 (eds. Papike and Merrill). Lunar Planetary Institute, Houston.

1551 Muehlberger, W.R., Hörz, F., Sevier, J.R., and Ulrich, G.E.: 1980, `Mission Objectives for
1552 Geological Exploration of the Apollo 16 Landing Site', in J.J. Papike and R.B. Merrill
1553 (eds.), Proc. Conf on the Lunar Highland Crust, Houston, Texas, 1979, Pergamon Press,
1554 New York, pp. 1–49.

1555 Mundil R., Renne P.R., Min K.K. and Ludwig, K.R., 2006. Resolvable miscalibration of the
1556 $^{40}Ar/^{39}Ar$ geochronometer. Eos Trans. AGU 87 (52) Fall Meeting Supplement, Abstract
1557 V21A-0543.

1558 Neal, C.R. and Taylor, L.A., 1992. Petrogenesis of mare basalts: A record of lunar volcanism.
1559 Geochimica et Cosmochimica Acta 56, 2177-2211.

1560 Nemchin A. A., Pidgeon R. T., Healy D., Grange M. L., Whitehouse M. J. and Vaughan J.,
1561 2009b. The comparative behavior of apatite-zircon U-Pb systems in Apollo 14 breccias:

1562 Implications for the thermal history of the Fra Mauro Formation. Meteorit. Planet. Sci.
1563 44, 1717-1734.

1564 Nemchin A. A., Pidgeon R. T., Whitehouse M. J., Vaughan J. P. and Meyer C., 2008. SIMS
1565 U–Pb study of zircon from Apollo 14 and 17 breccias: implications for the evolution of
1566 lunar KREEP. Geochim. Cosmochim. Acta 72, 668-689.

1567 Nemchin, A.A., Jeon, H., Bellucci, J.J., Timms, N.E., Snape, J.F., Kilburn, M.R.,
1568 Whitehouse, M.J., 2017. Pb-Pb ages of feldspathic clasts in two Apollo 14 breccia
1569 samples. Geochim. Cosmochim. Acta 217, 441–461.

1570 Norman M.D., Duncan R.A. and Huard J.J., 2006. Identifying impact events within the lunar
1571 cataclysm from ^{40}Ar–^{39}Ar ages and compositions of Apollo 16 impact melt rocks.
1572 Geochim. et Cosmochim. Acta 70, 6032–6049.

1573 Norman, M.D., Duncan, R.A., Huard, J.J., 2010. Imbrium provenance for the Apollo 16
1574 Descartes terrain: Argon ages and geochemistry of lunar breccias 67016 and 67455.
1575 Geochim. Cosmochim. Acta 74, 763–783.

1576 Papanastassiou D.A. and Wasserburg G.J., 1971. Rb-Sr ages of igneous rocks from the
1577 Apollo 14 mission and the age of the Fra Mauro formation. Earth Planet. Sci. Lett. 12,
1578 37–48.

1579 Papanastassiou D.A. and Wasserburg G.J., 1972a. The Rb-Sr age of a crystalline rock from
1580 Apollo 16. Earth Planet. Sci. Lett. 16, 289–298.

1581 Papanastassiou D.A. and Wasserburg G.J., 1972b. Rb-Sr systematics of Luna 20 and Apollo
1582 16 samples. Earth Planet. Sci. Lett. 17, 52–63.

1583 Papike, J.J., Simon, S.B. and Laul, J.C., 1982. The Lunar Regolith: Chemistry, mineralogy,
1584 and petrology. Reviews of Geophysics 20, 761-826.

1585 Reimold W.U., Nyquist L.E., Bansal B.M., Wooden J.L., Shih C.-Y., Weismann H. and
1586 Mackinnon I.D.R., 1985. Isotope analysis of crystalline impact melt rcks from Apollo 16
1587 Stations 11 and 13, North Ray Crater. Proc. Lunar Planet. Sci. Conf. 15th, J. Geophys.
1588 Res. 90 Suppl., C431–C448.

1589 Renne P.R., Swisher C.C., Deino A.L., Karner D.B., Owens T. and DePaolo D.J., 1998.
1590 Intercalibration of standards, absolute ages and uncertainties in $^{40}Ar/^{39}Ar$ dating. Chem.
1591 Geol. 145, 117–152.

1592 Renne, P.R., Mundil, R., Balco, G., Min, K., Ludwig, K.R., 2010. Joint determination of 40K
1593 decay constants and $^{40}Ar^*/^{40}K$ for the Fish Canyon sanidine standard, and improved
1594 accuracy for 40Ar/39Ar geochronology. Geochim. Cosmochim. Acta 74 (18),
1595 5349e5367.

1596 Ridley, W.I., 1975. On high-alumina mare basalts. Proc. Lunar Sci. Conf. 6th, 131-145.

1597 Ryder and Spudis, 1987. Chemical composition and origin of Apollo 15 impact melts. Proc.
1598 Lunar Planet. Sci. Conf. 17th in J. Geophys. Res. 92, E432–E446.

1599 Ryder G. and Norman M., 1980. Catalog of Apollo 16 rocks, 16904. NASA, Johnson Space
1600 Center Publication, 1144 pp.

1601 Ryder G., Stoeser D.B., Marvin U.B., Bower J.F. and Wood J.A., 1975. Boulder 1, Station 2,
1602 Apollo 17: Petrology and petrogenesis, Moon 14, 327–357.

1603 Ryder, G. and A. Wood, J., 1977. Serenitatis and Imbrium impact melts: Implications for
1604 large-scale layering in the lunar crust. Proc. Lunar Sci. Conf. 8th., 655-668.

1605 Ryder, G. and Bower, J.F., 1977. Petrology of Apollo 15 black-and-white rocks 15445 and
1606 15455 - Fragments of the Imbrium impact melt sheet, Lunar & Planetary Science
1607 Conference. Proc. 7th Lunar Sci. Conf. 1925-1948.

1608 Ryder, G., 1990. Lunar samples, lunar accretion and the early bombardment of the Moon.
1609 EOS Trans. 71, 313.

1610 Schaeffer O.A., Husain L. and Schaeffer G.A, 1976. Ages of highland rocks: The chronology
1611 of lunar basin formation revisited. Proc. Lunar Planet. Sci. Conf. 7th, 2067–2092.

1612 Schwarz W.H. and Trieloff M., 2007. Intercalibration of ^{40}Ar–^{39}Ar age standards NL-25,
1613 HB3gr hornblende, GA1550, SB-3, HD-B1 biotite and BMus/2 muscovite. Chem. Geol.
1614 242, 218–231.

1615 Shervais, J.W., Taylor, L.A. and Lindstrom, M.M., 1985. Apollo 14 Mare basalts: Petrology
1616 and geochemistry of clasts from Consortium Breccia 14321. Journal of Geophysical
1617 Research: Solid Earth 90, C375–C395.

1618 Simonds, C.H., Phinney, W.C., Warner, J.L., Mcgee, P.E., Geeslin, J., Brown, R.W. and
1619 Rhodes, J.M., 1977. Apollo 14 revisited, or breccias aren't so bad after all. Proc. Lunar
1620 Sci. Conf. 8th, 1869–1893.

Snape, J. F., Nemchin, A.A., Bellucci, J.J., Whitehouse, M.J., Tartèse, R., Barnes, J.J., Anand, M., Crawford, I.A., Joy, K.H., 2016b. Lunar basalt chronology, mantle differentiation and implications for determining the age of the Moon. Earth Planet. Sci. Lett. 451, 149–158.

Snape, J. F., Nemchin, A.A., Grange, M.L., Bellucci, J.J., Thiessen, F., Whitehouse, M.J., 2016a. Phosphate ages in Apollo 14 breccias: Resolving multiple impact events with high precision U-Pb SIMS analyses. Geochim. Cosmochim. Acta 174, 13–29.

Snape, J.F., Nemchin, A.A., Bellucci, J.J., Whitehouse, M.J., 2017. Pb isotopes in the impact melt breccia 66095: Association with the Imbrium basin and the isotopic composition of lithologies at the Apollo 16 landing site. Chem. Geol. 466, 608–616.

Spudis P.D. and Ryder G., 1981. Apollo 17 impact melts and their relation to the Serenitatis basin. Proc. Lunar Planet. Sci. Conf. 10th, 745–762.

Spudis, P. D., D. E. Wilhelms, M. S. Robinson, 2011. The Sculptured Hills of the Taurus Highlands: Implications for the relative age of Serenitatis, basin chronologies and the cratering history of the Moon. J. Geophys. Res. 116, E00H03.

Spudis, P., C. Pieters, 1991. Global and regional data about the Moon (Chapter 10), in: Heiken, G. H., Vaniman, D. T., French, B. M. (Eds.), Lunar Sourcebook: A Users Guide to the Moon. Cambridge University Press, Houston, pp. 595-632. Or Wilhelms, 1987.

Stacey J. S. and Kramers J. D., 1975. Approximation of terrestrial lead isotope evolution by a two-stage model. Earth Planet. Sci. Lett. 26, 207-221.

Stadermann F.J., Heusser E., Jessberger E.K., Lingner S. and Stöffler D., 1991. The case for a younger Imbrium basin: New ^{40}Ar-^{39}Ar ages of Apollo 14 rocks. Geochim. Cosmochim. Acta 55, 2339–2349.

Staudacher Th., Jessberger E.K., Flohs I. and Kirsten T., 1979. ^{40}Ar-^{39}Ar systematics of consortium breccia 73255. Proc. Lunar Planet. Sci. Conf. 10th, 745–762.

Steiger R.H. and Jäger E., 1977. Subcommission on Geochronology: Convention of the use of decay constants in geo- and cosmochronology. Earth Planet. Sci. Lett. 36, 359–362.

Stern, R., 2001. A new isotopic and trace-element standard for the ion microprobe: preliminary thermal ionization mass spectrometry (TIMS) U-Pb and electron-microprobe data. Ressources naturelles Canada, Ottawa.

1651 Stöffler, D., Knöll, H.D., Marvin, U.B., Simonds, C.H. and Warren, P.H., 1980)
1652 Recommended classification and nomenclature of lunar highland rocks - A committee
1653 report. Geochimica Et Cosmochimica Acta -1, 51-70.

1654 Stöffler D., Bode K.D., Jessberger E.K., Lingner S., Palme H., Spettel B., Stadermann F.J.,
1655 and Wänke H. (1989) Fra Mauro Formation, Apollo 14: IV Synopsis and Synthesis of
1656 Consortium Studies. In Workshop on the Moon in Transition: Apollo 14, KREEP and
1657 evolved rocks. (eds. Taylor and Warren) LPI Tech Rpt. 89-03, 145-148. Lunar Planetary
1658 Institute, Houston.

1659 Stöffler Dieter (1989) Brecciated nature of the Apollo 14 lunar samples: A review. In
1660 Workshop on the Moon in Transition: Apollo 14, KREEP and evolved rocks. (eds.
1661 Taylor and Warren) LPI Tech Rpt. 89-03, 138-144. Lunar Planetary Institute, Houston.

1662 Swann, G.A., Bailey, N.G., Batson, R.M., Eggleton, R.E., Hait, M.H., Holt, H.E., Larson,
1663 K.B., Reed, V.S., Schaber, G.G., Sutton, R.L., Trask, N.J., Ulrich, G.E., Wilshire, H.G.,
1664 1977. Geology of the Apollo 14 landing site in the Fra Mauro highlands. USGS Prof.
1665 Pap. 880, 103.

1666 Swann, G.A., Trask, N.J., Hait, M.H., Sutton, R.L., 1971. Geologic Setting of the Apollo 14
1667 Samples. Science 173, 716–719.

1668 Tera, F. and Wasserburg, G.J. (1973) A response to a comment on U-Pb systematics in lunar
1669 basalts. Earth Planet. Sci. Lett. 19, 213-217.

1670 Tera, F., Papanastassiou, D.A., Wasserburg, G.J., 1974. Isotopic evidence for a terminal lunar
1671 cataclysm. Earth Planet. Sci. Lett. 22, 1–21.

1672 Thiessen, F., Nemchin, A.A., Snape, J.F., Bellucci, J.J., Whitehouse, M.J., 2018. Apollo 12
1673 breccia 12013: Impact-induced partial Pb loss in zircon and its implications for lunar
1674 geochronology. Geochim. Cosmochim. Acta 230, 94–111.

1675 Thiessen, F., Nemchin, A.A., Snape, J.F., Whitehouse, M.J., Bellucci, J.J., 2017. Impact
1676 history of the Apollo 17 landing site revealed by U-Pb SIMS ages. Meteorit. Planet. Sci.
1677 52, 584–611.

1678 Timms NE, Erickson TM, Pearce MA, Cavosie AJ, Schmieder M, Tohver E, Reddy SM,
1679 Zanetti M, Nemchin AA, Wittmann A (2017) A pressure-temperature phase diagram for
1680 zircon at extreme conditions. Earth Science Reviews 165, 185-202

1681 Turner G. and Cadogan P.H. (1975b). The history of lunar bombardment inferred from ^{40}Ar-
1682 ^{39}Ar dating of highland rocks. Proc. Lunar Planet. Sci. Conf. 6th, 1509–1538.

1683 Turner G., Cadogan P.H. and Yonge C.J. (1973). Argon selenochronology. Proc. Lunar
1684 Planet. Sci. Conf. 4th, Suppl. 4, Geochim. Cosmochim. Acta, 1889–1914.

1685 Turner, G., Cadogan, P.H., Yonge, C.J., 1973. Argon selenochronology, in: Lunar and
1686 Planetary Science Conference Proceedings, Lunar and Planetary Science Conference
1687 Proceedings. pp. 1889–1914.

1688 Warner J.L. (1972). Metamorphism of Apollo 14 breccias. Proc. Lunar Planet. Sci. Conf. 3rd,
1689 Suppl. 3, Geochim. Cosmochim. Acta vol # 623–643.

1690 Warren, P. H., F. Ulff-Møller, G. W. Kallemeyn (2005) "New" lunar meteorites: Impact melt
1691 and regolith breccias and large-scale heterogeneities of the upper lunar crust. Meteorit.
1692 Planet. Sci. 40, 989-1014.

1693 Wilhelms, D. E. (1987) The geologic history of the Moon. U.S. Geol. Surv. Spec. Pap. 1348.

1694 Wilhelms, D.E. (1972) Reinterpretation of the northern Nectaris basin. Apollo 16 preliminary
1695 science report: NASA Report SP-315, chap. 29, part F, 29-27–29-30.

1696 Williams I S, 1998. U-Th-Pb geochronology by ion microprobe. In: McKibben M A, Shanks
1697 III W C, Ridley W I eds. Applications of Microanalytical Techniques to Understanding
1698 Mineralizing Processes. Rev Econ Geol. 7: 1-35.

1699 Williams R.J. (1972) The lithification of metamorphism of lunar breccias. Earth Planet. Sci.
1700 Lett. 16, 250-256.

1701 Wilshire H.G. and Jackson E.D. (1972b) Petrology and stratigraphy of the Fra Mauro
1702 Formation at the Apollo 14 site. US Geol. Survey Prof. Paper 785

1703 Winzer S.R., Nava D.F., Schuhmann P.J., Lum R.K.L., Schuhmann S., Lindstrom M.M.,
1704 Lindstrom D.J. and Philpotts J.A. (1977) The Apollo 17 "melt sheet": Chemistry age and
1705 Rb/Sr systematics. Earth Planet. Sci. Lett. 33, 389–400.

1706 Wittmann A, Kenkmann T, Schmitt RT, Stöffler D (2006) Shock-metamorphosed zircon in
1707 terrestrial impact craters. Meteorit. Planet. Sci. 41(3):433-454

1708 Woodhead, J.D., Hergt, J.M., 2000. Pb-Isotope Analyses of USGS Reference Materials.
1709 Geostand. Newsl. 24, 33–38.

Zhang A. C., Taylor L. A., Wang R. C., Li Q. L., Li X. H., Patchen A. D. and Liu Y. (2012) Thermal history of Apollo 12 granite and KREEP-rich rock: Clues from Pb/Pb ages of zircon in lunar breccia 12013. Geochim. Cosmochim. Acta 95, 1-14.

Zhang, B., Lin, Y., Moser, D., Hao, J., Shieh, S., and Bouvier A. (2019). Imbrium age for zircons in Apollo 17 South Massif impact melt breccia 73155. J. Geophys. Res. 124, 3205-3218.

Figure captions

Figure 1. U-Pb phosphate data from Apollo 12 and 14 samples investigated by Thiessen et al. (2017) and Snape et al. (2016a) shown using inverted Tera-Wasserburg diagrams (Tera and Wasserburg, 1973). A, B, and C –sample 12013; D, E, and F – sample 14305; G, I, and K – sample 14314. Terrestrial Pb composition (SK) corresponds to modern Pb determined from the Stacey and Kramers (1975) model; lunar initial Pb composition defined by Nemchin et al. (2017); the composition determined by Snape et al. (2017) for the Apollo 16 site is also shown in A. Red arrows in A and B indicate trajectory of lunar initial Pb correction, with the resulting corrected compositions indicated either by a red cross (A) or ellipse (B). Dashed blue lines in A, D, and E are best fit lines determined from uncorrected analyses (red curves represent error envelopes). Red crosses and ellipses in G, I, and K show analyses of a single grain in 14314, giving consistently older ages than the rest of the analyses. A, B, D, E, G, and I show uncorrected data; C, F, and K – the data corrected for compositions defined from the best-fit intercepts with the mixing line between "SK" and "Lunar Pb".

Figure 2. Pb-Pb data for VHK clasts from the sample 14305. (A) $^{207}Pb/^{206}Pb$ vs $^{204}Pb/^{206}Pb$ diagram; Error cross colors represent different clasts (grey– clast 1; red– clast 2; green– clast 3; blue– clast 4; light blue– clast 5), while circles indicate data points used to define lines representing different two-component mixtures (red– pure lunar Pb, defining an isochron; black: line between contamination and lunar initial Pb; light blue: between in-situ accumulated Pb and contamination; SK: modern Pb of Stacey and Kramers (1975). (B) $^{208}Pb/^{206}Pb$ vs. $^{204}Pb/^{206}Pb$ diagram; symbols are similar to those in A.

Figure 3. U-Pb data for Apollo 15 samples. (A) $^{207}Pb/^{206}Pb$ vs. $^{204}Pb/^{206}Pb$ diagram with the best fit line through the uncorrected analytical data points for apatite from 15455,62 (red crosses) and 15455,30 (black crosses) passing through SK composition and defining the age

of the samples. (B) $^{207}Pb/^{206}Pb$ vs $^{238}U/^{206}Pb$ diagram showing data corrected for non in-situ Pb; colour of ellipses similar to A. (C) weighted average of corrected $^{207}Pb/^{206}Pb$ ages

Figure 4. Examples of zircon and phosphate grains from the fragment 14161,7125. (A) Largest (about 50 μm) zircon grain found in the fragment (Zr1). Some boundaries with the surrounding crystallized impact melt, composed of pyroxene and plagioclase appear to be straight, while one of the boundaries forms embayments penetrated by the pyroxene – plagioclase assemblage; (B) Small subhedral zircon grain (Zr2) similar in size to the average size of the surrounding pyroxene and plagioclase crystals. Group of smaller elongated zircon grains also visible in the lower part of the image, appearing to be an integral part of impact melt assemblage; (C) Two zircon (Zr3, Zr4) and apatite/merrillite grains (Apt2, Apt-Mer composite grain). Zircon grains have subrounded boundaries with the surrounding assemblage. Apatite/merrillite grain is angular and straight boundary between apatite and merrillite is cut by the outer termination of the grain, suggesting that this grain was inherited from the target; (D) Zircon (Zr5) shows irregular boundaries with the surrounding assemblage; (E) elongated zircon grain (Zr6), which could be interpreted as a fragment reworked by the melt; (F) group of small zircon grains (Zr7), which are likely to have crystallized as part of the impact melt mineral assemblage; (G) zircon (Zr8) showing crystallographic faces on one side and an irregular boundary on the other; (H) large (more than 100 μm) apatite grain (Apt1) with irregular boundaries, indicating that it was inherited from the target of the impact that formed the impact melt.

Figure 5. U-Pb zircon data for three impact-melt fragments from sample 14161. (A) 14161,7125; (B) 14161,7233; (C) 14161,7060.

Figure 6. U-Pb apatite data for the fragment 14161,7125. (A) $^{207}Pb/^{206}Pb$ vs. $^{204}Pb/^{206}Pb$ diagram showing the best fit line through the uncorrected analytical data points passing between SK and lunar Pb compositions and defining age of the sample. Analytical data are hardly visible at this scale and all concentrated in the lower left corner of the diagram; (B) Zoomed $^{207}Pb/^{206}Pb$ vs. $^{204}Pb/^{206}Pb$ plot showing distribution of analytical points relative to the best fit line; (C) $^{207}Pb/^{206}Pb$ vs. $^{238}U/^{206}Pb$ diagram showing data corrected for non in-situ Pb; (D) weighted average of corrected $^{207}Pb/^{206}Pb$ ages.

Figure 7. BSE images of zircon and phosphate grains from the impact melt fragment 14161,7233. (A) four larger zircon grains are labelled in the image, multiple smaller euhedral grains showing similar BSE contrast are also zircon grains. (B) two granular zircon grains.

(C) elongated apatite grain similar in size to coexisting pyroxene and plagioclase grains. (D) merrillite grains.

Figure 8. U-Pb apatite (red symbols) and merrillite (black symbols) data for the fragment 14161,7233. (A) $^{207}Pb/^{206}Pb$ vs $^{204}Pb/^{206}Pb$ diagram with the best fit line through the six uncorrected analyses. (B) Zoomed $^{207}Pb/^{206}Pb$ vs. $^{204}Pb/^{206}Pb$ plot showing distribution of analytical points relative to the best fit line. Red dots indicate data used to constrain this line; (C) $^{207}Pb/^{206}Pb$ vs $^{238}U/^{206}Pb$ diagram showing data corrected for non in-situ Pb. (D) weighted average of corrected $^{207}Pb/^{206}Pb$ ages.

Figure 9. U-Pb merrillite data for the fragment 14161,7060. (A) $^{207}Pb/^{206}Pb$ vs $^{204}Pb/^{206}Pb$ diagram with the best fit line through the uncorrected analyses. (B) Zoomed $^{207}Pb/^{206}Pb$ vs. $^{204}Pb/^{206}Pb$ plot showing distribution of analytical points relative to the best fit line. (C) $^{207}Pb/^{206}Pb$ vs $^{238}U/^{206}Pb$ diagram showing data corrected for non in-situ Pb. (D) weighted average of corrected $^{207}Pb/^{206}Pb$ ages.

Figure 10. Median age of Apollo 14 samples with the limits determined from external variability of available ages shown as standard box-and-whisker diagram. All other samples with the ages around 3.9 Ga are plotted with their internal errors, indicating no statistical difference from the median age defined by Apollo 14 samples. Data for: Apollo 14 from this study and Snape et al. (2016a); Apollo 15 from this study; Apollo 16 from Snape et al. (2017); Apollo 17 from Thiessen et al. (2017a) and Grange et al. (2009); Apollo 12 from Thiessen et al. (2017b) and Liu et al. (2012); Sau169 from Liu et al. (2012)

Figure 11. Median of ages of all samples from five landing sites combined shown as standard box-and-whisker diagram. Phosphate data from 14321 and 14311 are also shown for comparison, indicating possibility that phosphates from these two samples can be marginally older that the best Imbrium age determined from all other samples. Combined data for Apollo 14 is from this study and Snape et al. (2016a); Data for 14321 is from Snape et al. (2016a) and data for 14311 is from Merle et al. (2014)

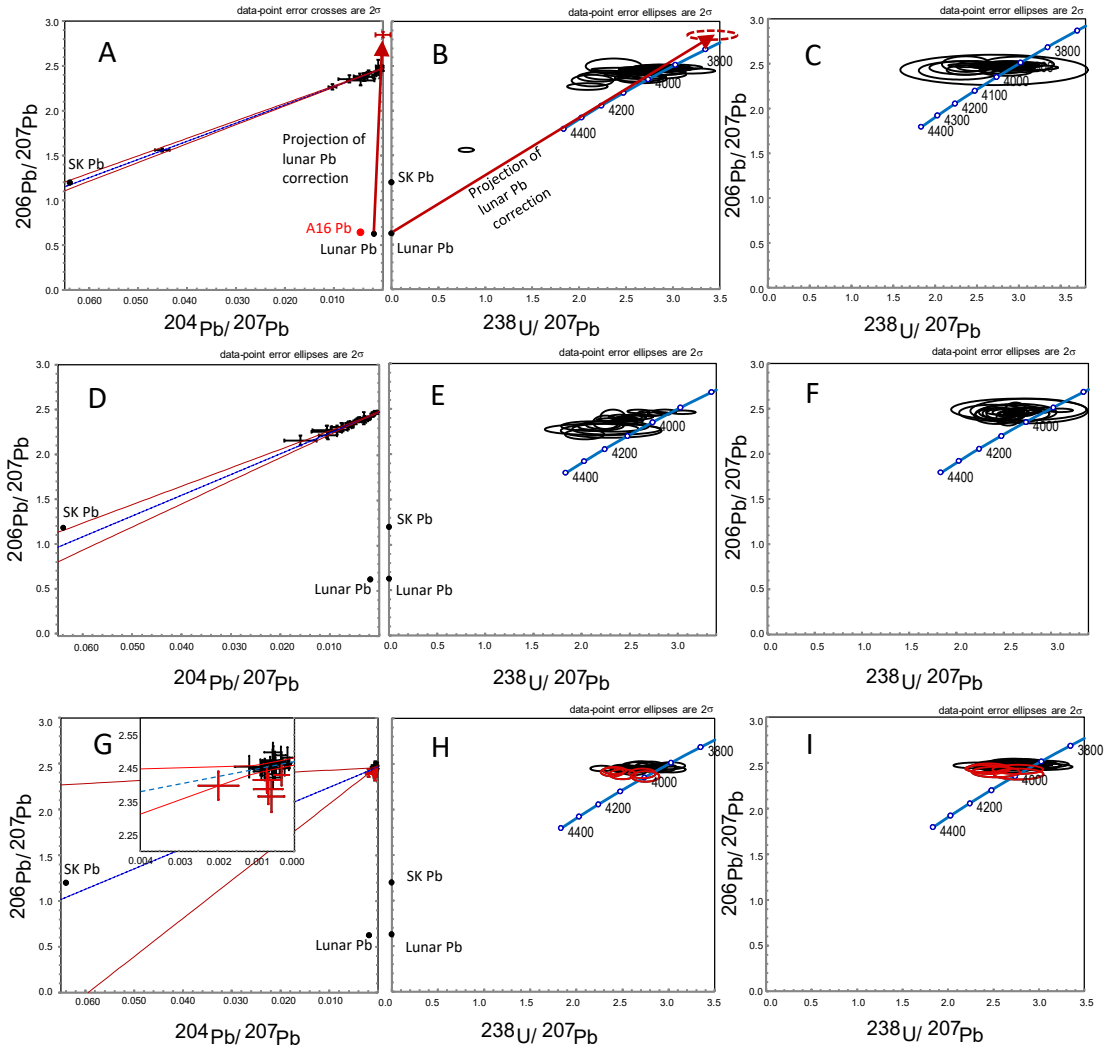
data-point error crosses are 2σ
A
SK Pb
Projection of lunar Pb correction
A16 Pb
Lunar Pb
$^{206}Pb/^{207}Pb$
$^{204}Pb/^{207}Pb$
data-point error ellipses are 2σ
B
SK Pb
Projection of lunar Pb correction
Lunar Pb
3800
4000
4200
4400
$^{238}U/^{207}Pb$
C
4100
4300
D
E
F
G
H
I

Figure 1

Figure 2

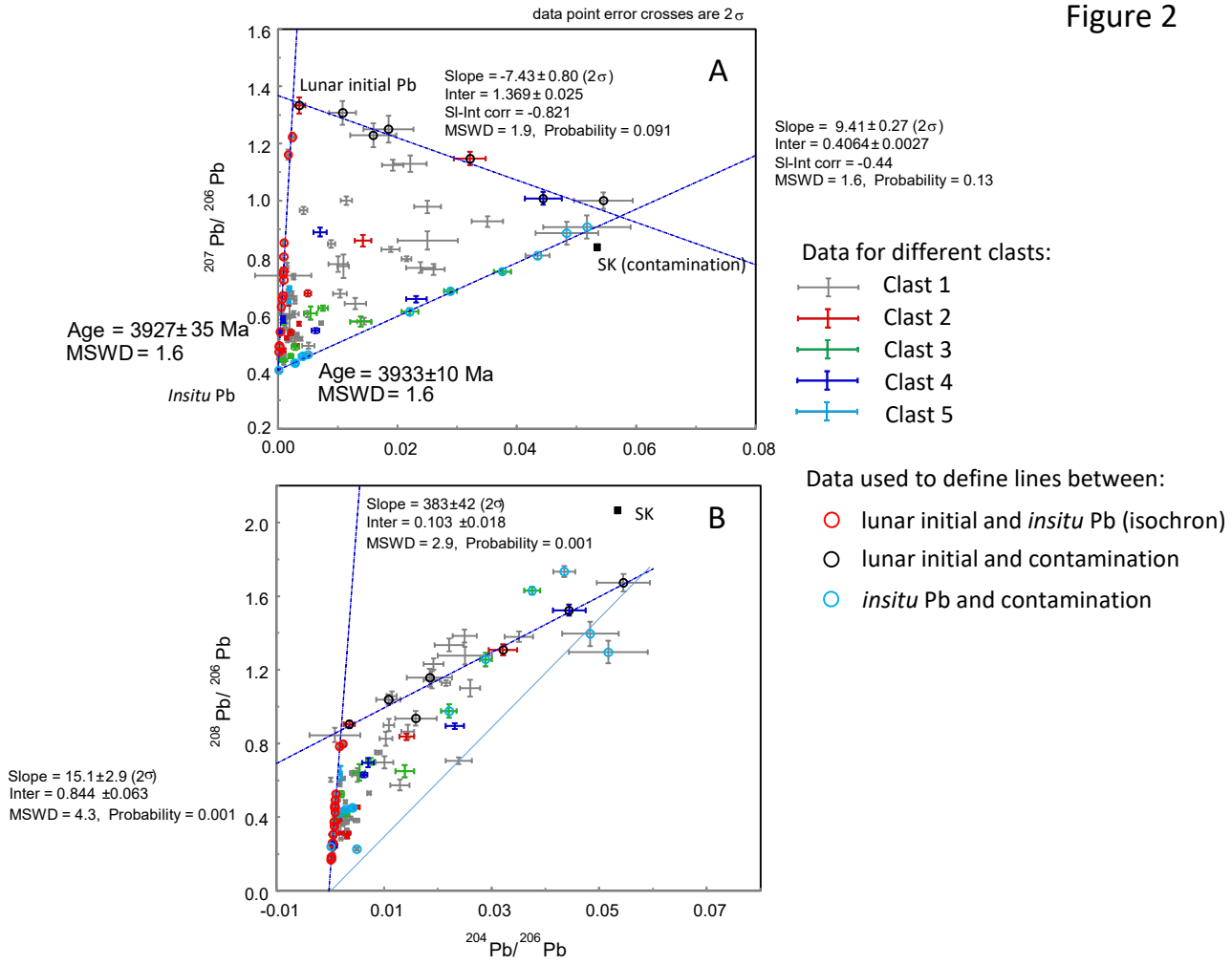
data point error crosses are 2σ
A
Lunar initial Pb
Slope = -7.43 ± 0.80 (2σ)
Inter = 1.369 ± 0.025
Sl-Int corr = -0.821
MSWD = 1.9, Probability = 0.091
SK (contamination)
Age = 3927± 35 Ma
MSWD = 1.6
Insitu Pb
Age = 3933±10 Ma
MSWD = 1.6
207 Pb/ 206 Pb
Slope = 9.41 ± 0.27 (2σ)
Inter = 0.4064 ± 0.0027
Sl-Int corr = -0.44
MSWD = 1.6, Probability = 0.13
Data for different clasts:
Clast 1
Clast 2
Clast 3
Clast 4
Clast 5
B
Slope = 383±42 (2σ)
Inter = 0.103 ±0.018
MSWD = 2.9, Probability = 0.001
SK
208 Pb/ 206 Pb
Slope = 15.1±2.9 (2σ)
Inter = 0.844 ±0.063
MSWD = 4.3, Probability = 0.001
204 Pb/ 206 Pb
Data used to define lines between:
lunar initial and insitu Pb (isochron)
lunar initial and contamination
insitu Pb and contamination

Figure 3

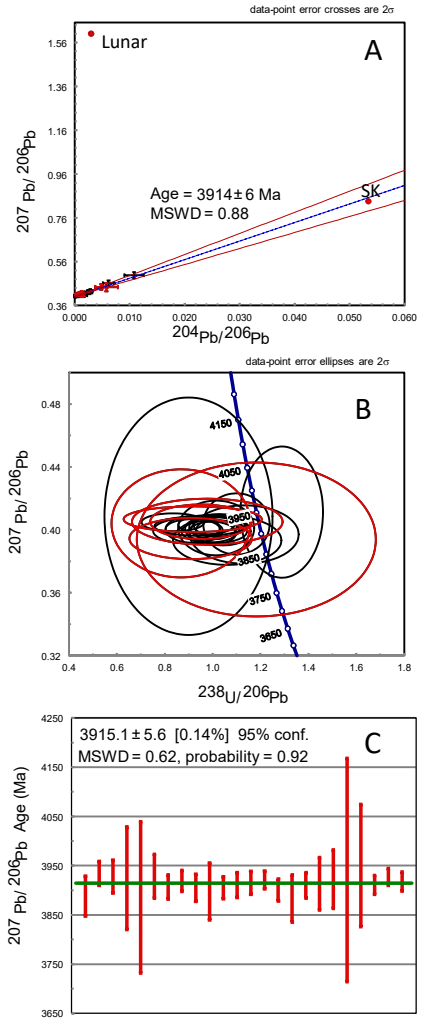
data-point error crosses are 2σ
Lunar
A
Age = 3914 ± 6 Ma
MSWD = 0.88
SK
207 Pb/ 206Pb
204Pb/206Pb
data-point error ellipses are 2σ
B
4150
4050
3950
3850
3750
3650
238U/206Pb
3915.1 ± 5.6 [0.14%] 95% conf.
MSWD = 0.62, probability = 0.92
C
207 Pb/ 206Pb Age (Ma)

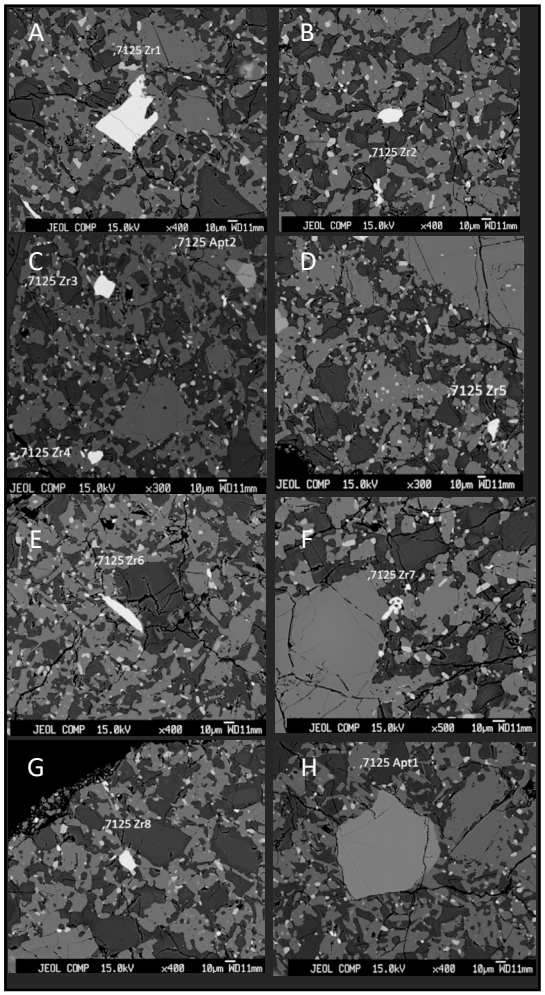
A
7125 Zr1
JEOL COMP 15.0kV ×400 10μm WD11mm
B
7125 Zr2
JEOL COMP 15.0kV ×400 10μm WD11mm
C
7125 Apt2
7125 Zr3
7125 Zr4
JEOL COMP 15.0kV ×300 10μm WD11mm
D
7125 Zr5
JEOL COMP 15.0kV ×300 10μm WD11mm
E
7125 Zr6
JEOL COMP 15.0kV ×400 10μm WD11mm
F
7125 Zr7
JEOL COMP 15.0kV ×500 10μm WD11mm
G
7125 Zr8
JEOL COMP 15.0kV ×400 10μm WD11mm
H
7125 Apt1
JEOL COMP 15.0kV ×400 10μm WD11mm

Figure 4

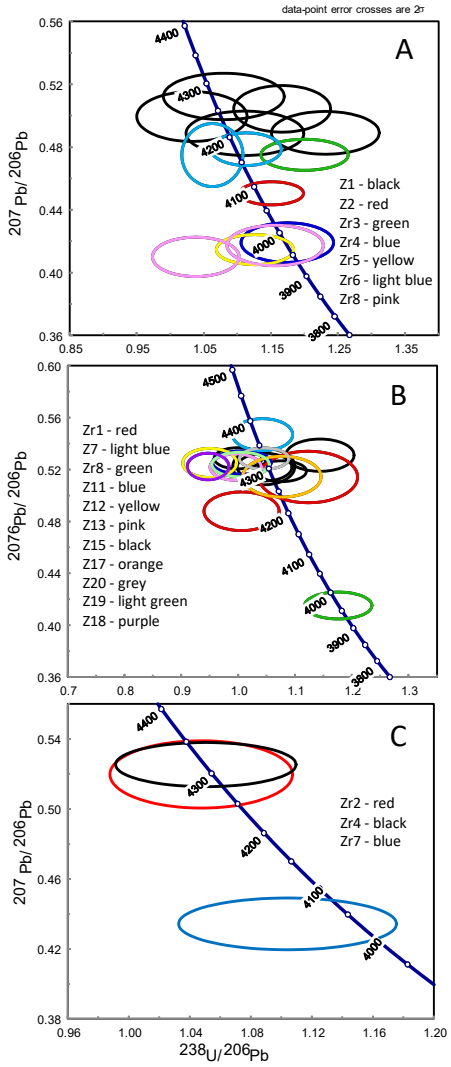
data-point error crosses are 2σ
A
Z1 - black
Z2 - red
Zr3 - green
Zr4 - blue
Zr5 - yellow
Zr6 - light blue
Zr8 - pink
B
Zr1 - red
Z7 - light blue
Zr8 - green
Z11 - blue
Z12 - yellow
Z13 - pink
Z15 - black
Z17 - orange
Z20 - grey
Z19 - light green
Z18 - purple
C
Zr2 - red
Zr4 - black
Zr7 - blue
207 Pb/ 206Pb
2076Pb/ 206Pb
238U/ 206Pb

Figure 5

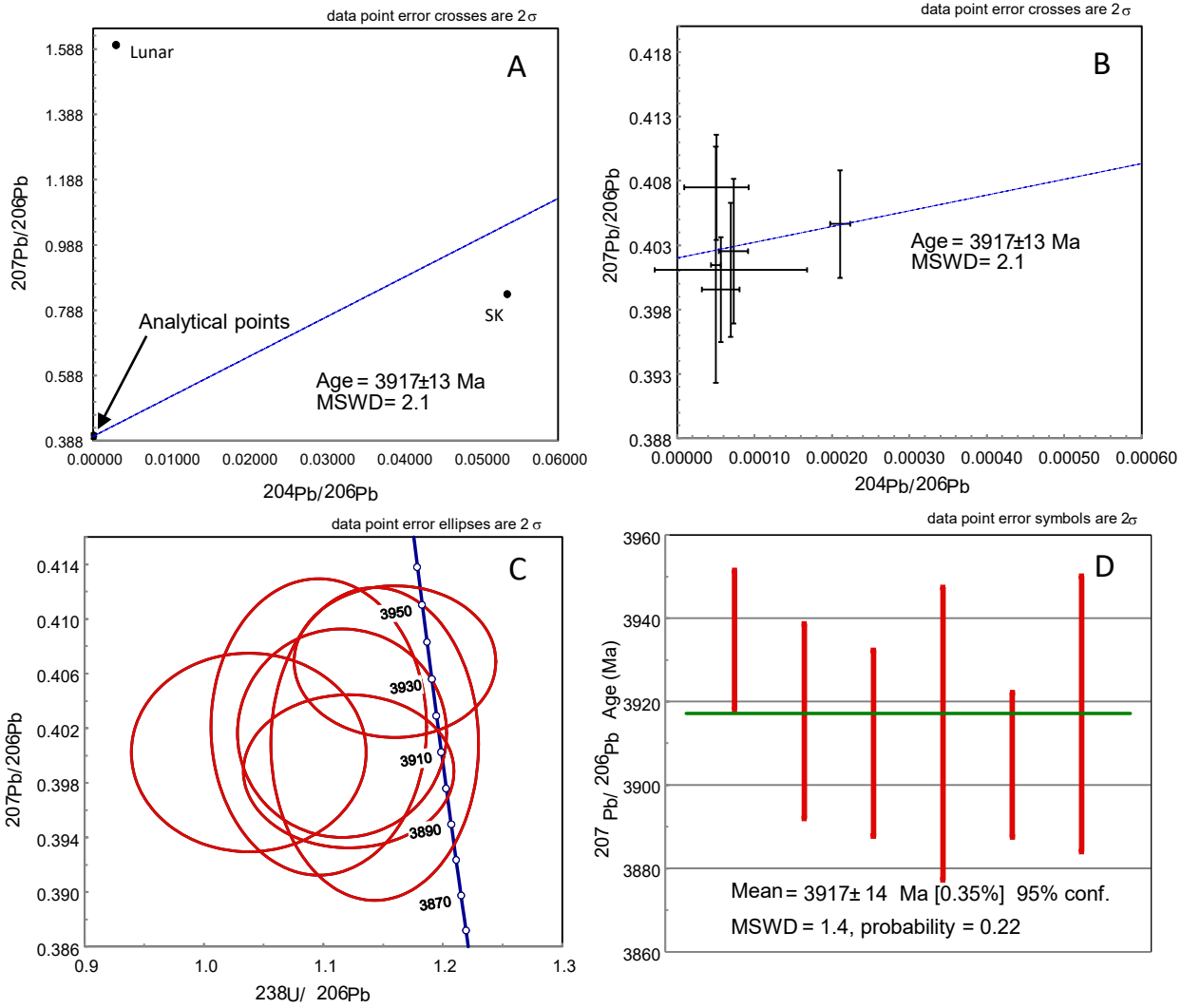
data point error crosses are 2σ
A
Lunar
SK
Analytical points
Age = 3917±13 Ma
MSWD= 2.1
207Pb/206Pb
204Pb/206Pb
1.588
1.388
1.188
0.988
0.788
0.588
0.388
0.00000
0.01000
0.02000
0.03000
0.04000
0.05000
0.06000
data point error crosses are 2σ
B
Age = 3917±13 Ma
MSWD= 2.1
207Pb/206Pb
204Pb/206Pb
0.418
0.413
0.408
0.403
0.398
0.393
0.388
0.00000
0.00010
0.00020
0.00030
0.00040
0.00050
0.00060
data point error ellipses are 2 σ
C
3950
3930
3910
3890
3870
207Pb/206Pb
238U/ 206Pb
0.414
0.410
0.406
0.402
0.398
0.394
0.390
0.386
0.9
1.0
1.1
1.2
1.3
data point error symbols are 2σ
D
Mean = 3917± 14 Ma [0.35%] 95% conf.
MSWD = 1.4, probability = 0.22
207 Pb/ 206Pb Age (Ma)
3960
3940
3920
3900
3880
3860

Figure 6

Figure 7

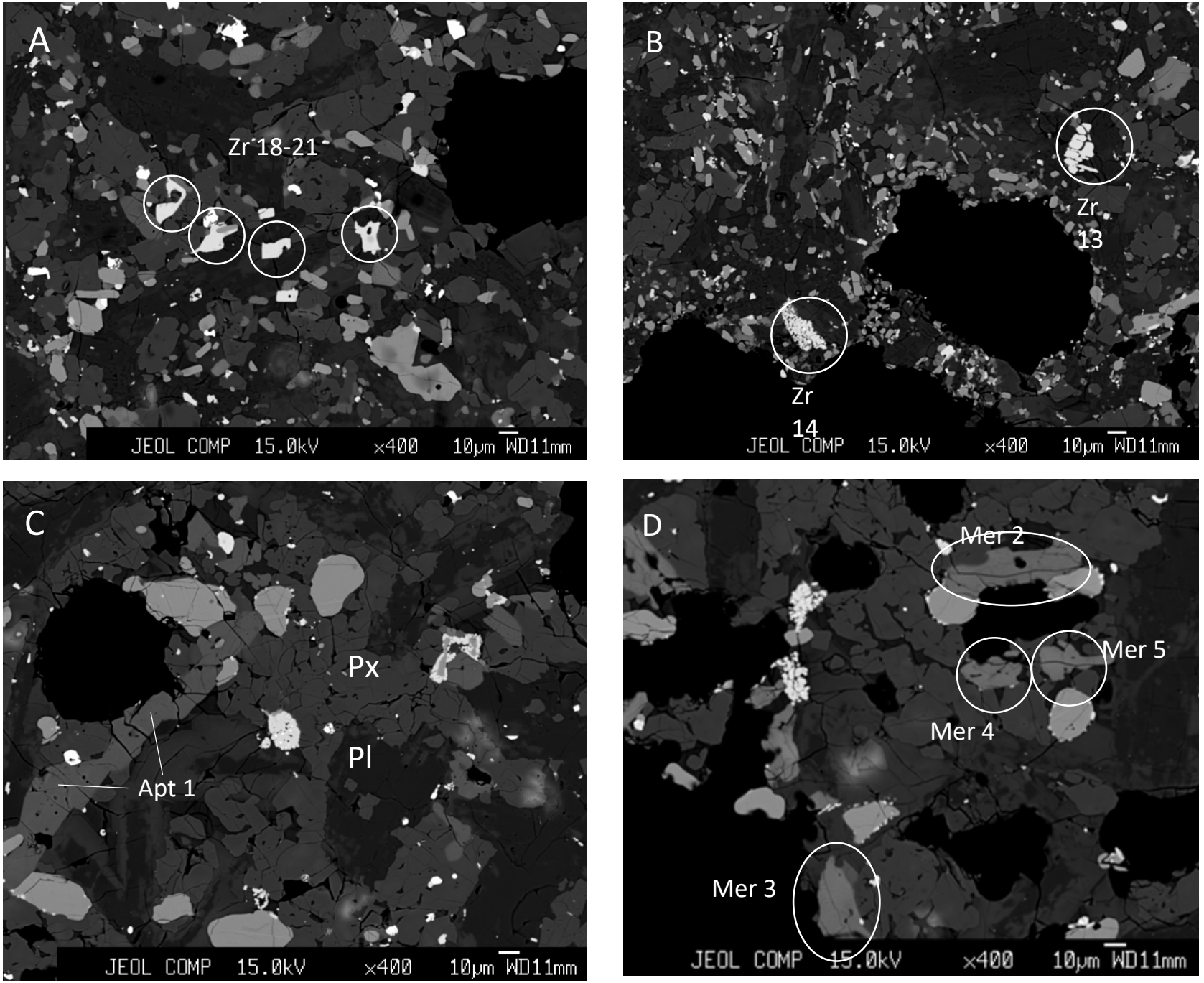
A
Zr 18-21
JEOL COMP 15.0kV ×400 10µm WD11mm
B
Zr 13
Zr 14
JEOL COMP 15.0kV ×400 10µm WD11mm
C
Px
Pl
Apt 1
JEOL COMP 15.0kV ×400 10µm WD11mm
D
Mer 2
Mer 5
Mer 4
Mer 3
JEOL COMP 15.0kV ×400 10µm WD11mm

Figure 8

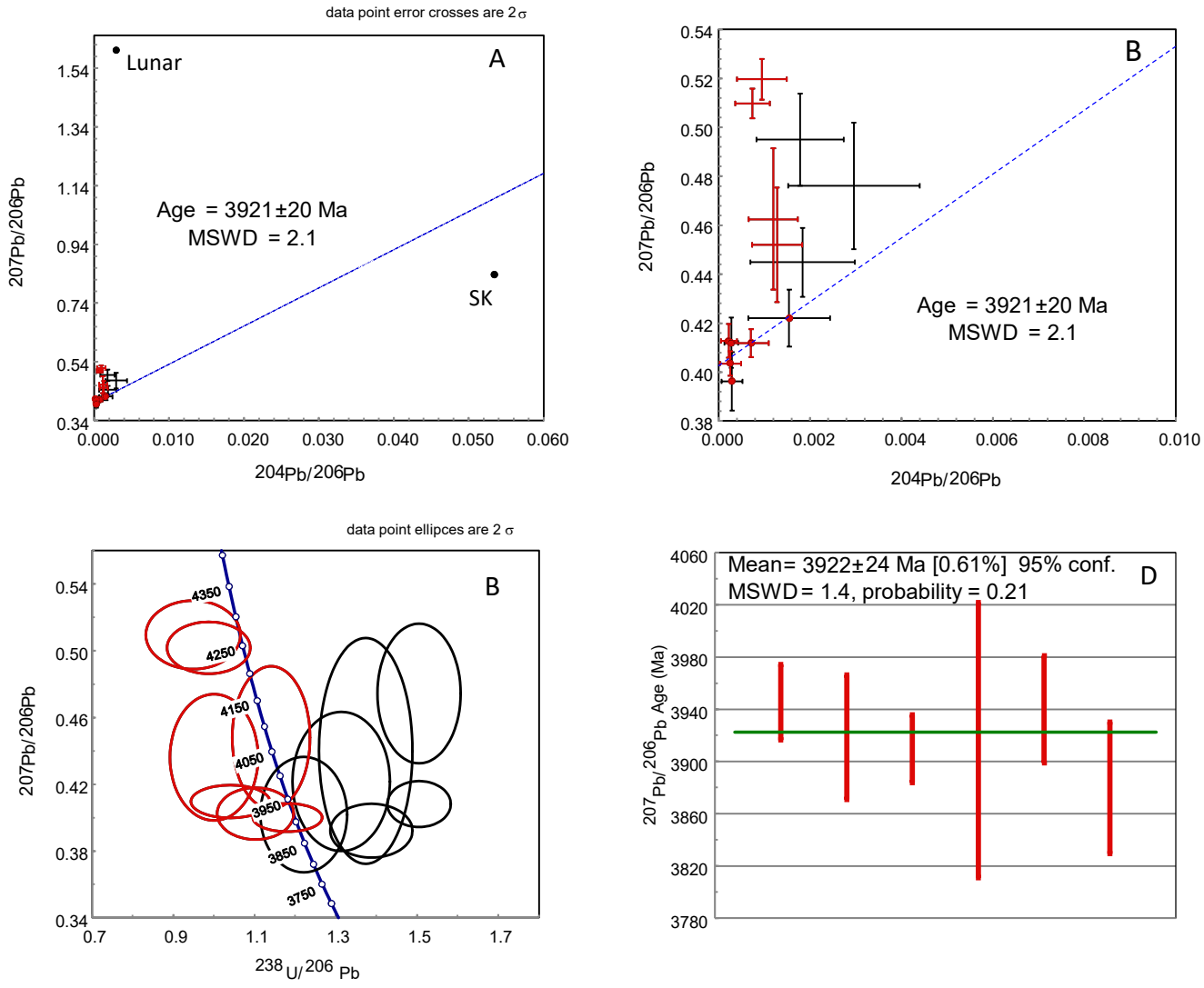
data point error crosses are 2 σ
Lunar
A
Age = 3921±20 Ma
MSWD = 2.1
SK
207Pb/206Pb
204Pb/206Pb
1.54
1.34
1.14
0.94
0.74
0.54
0.34
0.000
0.010
0.020
0.030
0.040
0.050
0.060
B
Age = 3921±20 Ma
MSWD = 2.1
0.54
0.52
0.50
0.48
0.46
0.44
0.42
0.40
0.38
0.002
0.004
0.006
0.008
0.010
data point ellipces are 2 σ
B
4350
4250
4150
4050
3950
3850
3750
0.7
0.9
1.1
1.3
1.5
1.7
238U/206Pb
Mean= 3922±24 Ma [0.61%] 95% conf.
MSWD= 1.4, probability = 0.21
D
207Pb/206Pb Age (Ma)
4060
4020
3980
3940
3900
3860
3820
3780

Figure 9

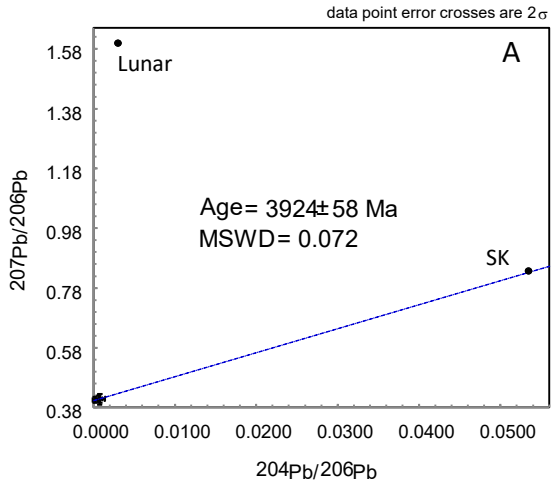
data point error crosses are 2σ
A
Lunar
SK
Age= 3924±58 Ma
MSWD= 0.072
207Pb/206Pb
204Pb/206Pb
1.58
1.38
1.18
0.98
0.78
0.58
0.38
0.0000
0.0100
0.0200
0.0300
0.0400
0.0500

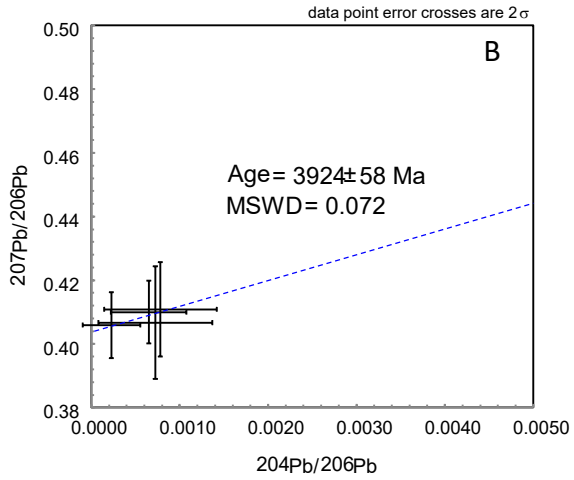
data point error crosses are 2σ
B
Age= 3924±58 Ma
MSWD= 0.072
207Pb/206Pb
204Pb/206Pb
0.50
0.48
0.46
0.44
0.42
0.40
0.38
0.0000
0.0010
0.0020
0.0030
0.0040
0.0050

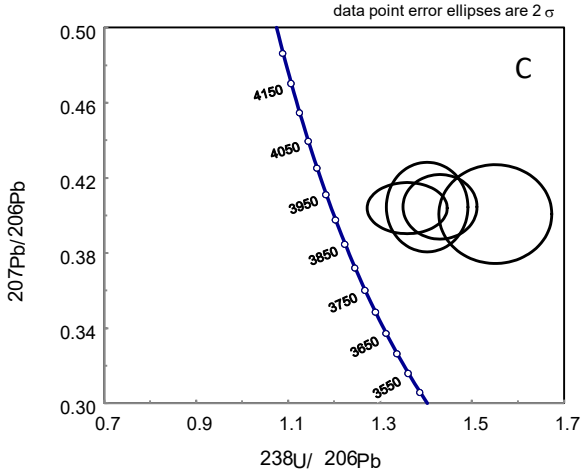
data point error ellipses are 2σ
C
4150
4050
3950
3850
3750
3650
3550
207Pb/206Pb
238U/ 206Pb
0.50
0.46
0.42
0.38
0.34
0.30
0.7
0.9
1.1
1.3
1.5
1.7

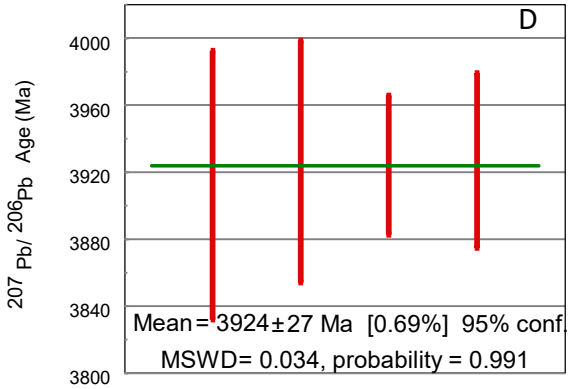
D
207 Pb/ 206Pb Age (Ma)
Mean=3924±27 Ma [0.69%] 95% conf.
MSWD= 0.034, probability = 0.991
4000
3960
3920
3880
3840
3800

Figure 10

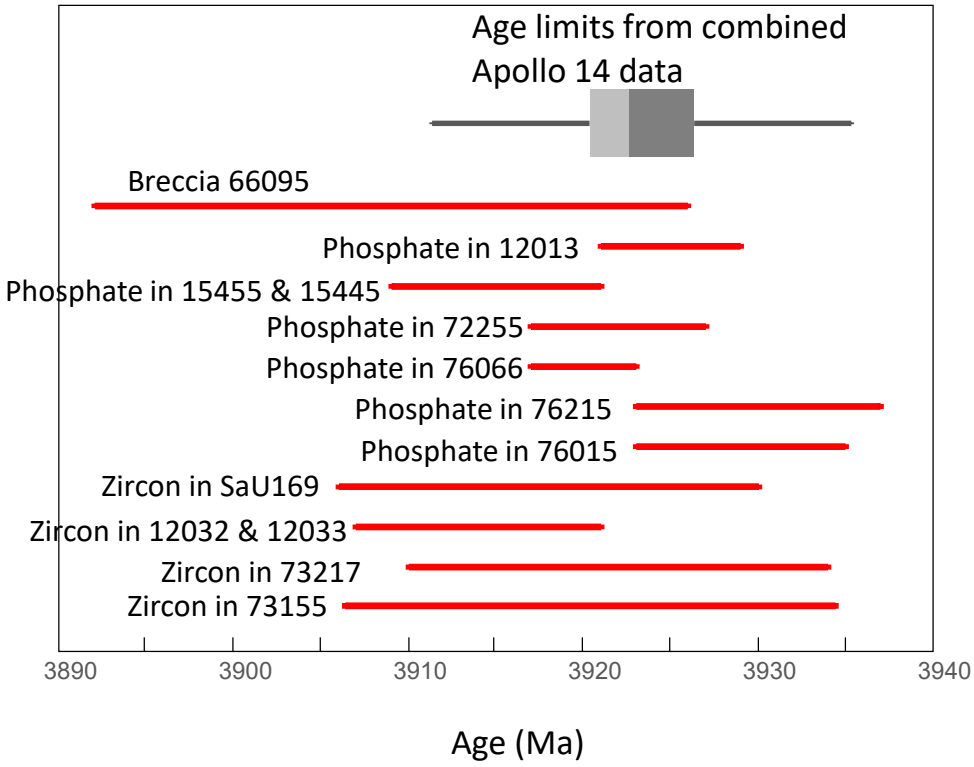
Age limits from combined
Apollo 14 data
Breccia 66095
Phosphate in 12013
Phosphate in 15455 & 15445
Phosphate in 72255
Phosphate in 76066
Phosphate in 76215
Phosphate in 76015
Zircon in SaU169
Zircon in 12032 & 12033
Zircon in 73217
Zircon in 73155
3890
3900
3910
3920
3930
3940
Age (Ma)

Figure 11

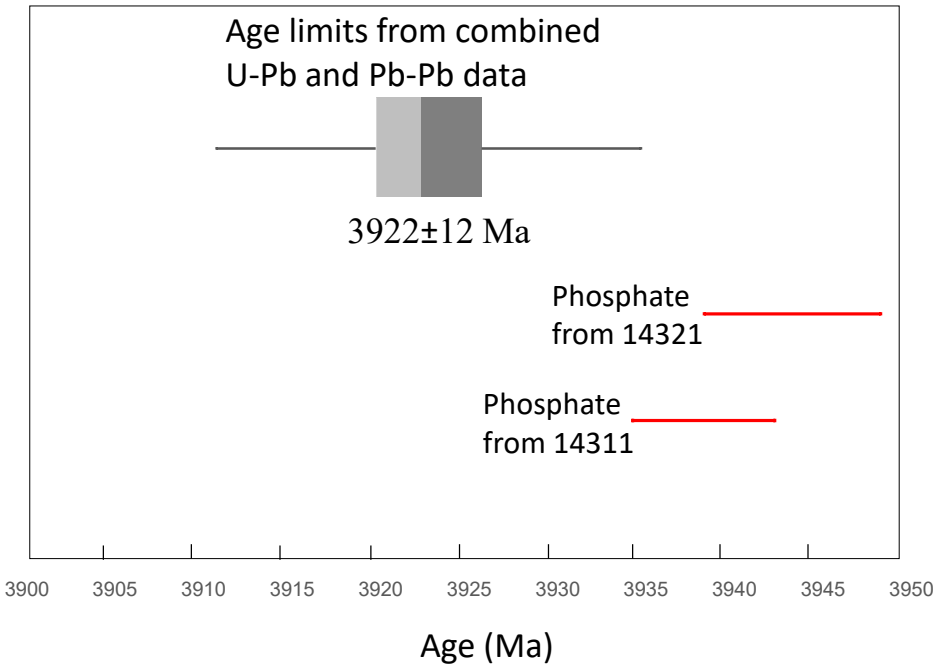
Age limits from combined
U-Pb and Pb-Pb data
3922±12 Ma
Phosphate
from 14321
Phosphate
from 14311
3900
3905
3910
3915
3920
3925
3930
3935
3940
3945
3950
Age (Ma)